POLITECNICO DI TORINO

Collegio di Ingegneria Chimica e dei Materiali

Corso di Laurea Magistrale in Ingegneria Chimica e dei Processi Sostenibili

Tesi di Laurea Magistrale

Computational Particle Fluid Dynamics (CPFD): Simulation of Pulsed Fluidized Beds





Relatori

Dr. Amblard Benjamin

Dr. Haroun Yacine

Dr. Lavalle Gianluca

Dr. Massaro Sousa Lucas

Dr. Specchia Stefania

Candidato

Roberto Scollo

Settembre 2025

1 Prefazione

Il presente lavoro investiga l'utilizzo della Computational Particle Fluid Dynamics (CPFD) per la simulazione di letti fluidizzati pulsanti, con un'attenzione in particolare sulla loro applicazione nel processo di Cracking Catalitico (Fluid Catalitic Cracking FCC) nella raffinazione del petrolio. Vengono allora integrati una revisione della letteratura a riguardo, una validazione sperimentale su impianto pilota e delle simulazioni numeriche in modo da garantire una panoramica dello stato dell'arte della tecnologia e una metodologia applicata per lo studio dell'impatto e la quantificazione dei benefici della pulsazione sulla fluidodinamica interna al letto fluidizzato.

1.1 Contesto

1.1.1 Cracking Catalitico (FCC)

Lo studio comincia con la descrizione del processo di Cracking Catalitico, uno dei processi principali all'interno della raffineria. A partire dal gasolio pesante in uscita dal fondo della colonna di distillazione atmosferica, il processo porta alla scissione di queste molecole e alla formazione di una miscela di alcani e alcheni C5-C11 e di aromatici con elevato numero di ottano, aumentando di fatto la resa del greggio in idrocarburi nel range della benzina.

Il reattore nel quale avviene la reazione prende il nome di "riser" ed è caratterizzato dal trasporto pneumatico delle particelle di catalizzatore per mezzo della portata di alimentazione vaporizzata. All'uscita del riser, i prodotti vengono separati dal catalizzatore per mezzo di cicloni, tuttavia, una parte di questi rimane intrappolata nei pori del solido, rendendo necessario un processo di stripping. Lo strippaggio avviene tramite l'invio di vapore in controcorrente al solido, creando un letto fluidizzato capace di aumentare l'efficienza di mixing e il trasporto di calore e di materia.

Questo studio si concentra sulla sezione di stripping del processo di FCC.

1.1.2 Letti Fluidizzati

I reattori a letto fluidizzato prevedono il passaggio di una corrente fluida attraverso un letto di solidi. Una volta raggiunta una velocità superficiale minima, chiamata velocità di minima fluidizzazione, il letto comincia a comportarsi come un fluido, da cui deriva una miscelazione più spinta e, dunque, un miglior controllo della temperatura (essenziale per reazioni fortemente endotermiche o esotermiche) e coefficienti di trasporto di materia e calore più elevati.

Tuttavia, la loro prevedibilità (da un punto di vista idrodinamico) e scalabilità è fortemente influenzata dal tipo di solido e dal regime fluidodinamico impiegati. In particolare, il catalizzatore FCC appartiene al gruppo A nella classificazione dei solidi di Geldart, per la quale le particelle sono classificate in base alla loro densità apparente e al loro diametro. Questi solidi presentano alcune instabilità, difficili da prevedere, nel loro moto all'interno della colonna a causa delle grandi forze di coesione interparticellari e della maggiore tendenza alla formazione di agglomerati. Ne conseguono maggiori difficoltà nello scale-up, disomogeneità interne al reattore e una ridotta efficienza di contatto tra le due fasi, fluida e solida.

1.1.3 Intensificazione di Processo e Pulsazione della Portata di Gas

L'intensificazione di processo nel caso dei letti fluidizzati si focalizza maggiormente sull'aumento della capacità di mixing, sulla riduzione della dimensione delle bolle e sulla stabilizzazione idrodinamica del reattore.

Tra le differenti tecniche sviluppate, l'aggiunta di una pulsazione alla corrente fluida in ingresso al letto si è dimostrata una tecnica non intrusiva e facile da implementare, generalizzabile a reattori con differenti geometrie e dimensioni e con un impatto positivo sull'efficienza del processo. Diversi studi hanno infatti trovato: una riduzione della velocità di minima fluidizzazione, un miglior controllo del reattore e più alti coefficienti di trasferimento; permettendo una riduzione della portata di fluido a parità di rendimento e dunque un costo e un impatto ambientale più bassi.

Da un punto di vista industriale, tuttavia, trova ancora una ridotta applicazione per via dell'inerzia del settore nel cambio degli strumenti di processo e per la mancanza di strumenti di simulazione sistematici e affidabili.

1.1.4 Contributo di IFPEN

IFP Energies Nouvelles è stato in grado di riconoscere le grandi capacità di risparmio energetico, in linea con le più recenti direttive in ambito ambientale e ha iniziato a condurre studi sperimentali su un impianto pilota.

L'obiettivo degli esperimenti era quello di valutare l'effetto della pulsazione, con frequenza tra gli 1 e i 7 Hz, sulla fluidodinamica e sul trasferimento di massa in un reattore a letto fluidizzato circolante, che riproducesse la sezione di stripping del processo di cracking.

Le misure di densità e altezza del letto, insieme alla valutazione delle quantità di un tracciante (Elio) ritrovate all'uscita dello stripper hanno sottolineato il potenziale di questa tecnica sulle performance del processo di stripping e fornito una base di dati sperimentali per la validazione del modello numerico implementato in questo studio.

1.1.5 Modelli Numerici

La terza sezione dell'elaborato fornisce una discussione approfondita sulle differenti strategie disponibili per la modellazione di sistemi bifasici e in particolare per la rappresentazione di letti fluidizzati gas-solido.

A causa della natura multiscala delle interazioni tra le due fasi e tra le particelle, i modelli multifase si presentano molto complessi e le tecniche tradizionali di CFD spesso fanno difficoltà a rappresentare correttamente questi fenomeni. Differenti approcci sono stati realizzati; questi, oltre alla Direct Numerical Simulation, vengono divisi in Euleriani-Euleriani e Euleriani-Lagrangiani, a seconda della strategia usata per la modellazione della fase gassosa e di quella solida, rispettivamente.

I modelli Euleriani-Euleriani trattano entrambe le fasi come fluidi utilizzando la Teoria Cinetica dei Flussi Granulari (KTGF) per la fase solida. Questi spesso forniscono risultati relativamente lontani dalla realtà o, in ogni caso, necessitano un adattamento dei parametri di simulazione che possono portare a costi computazionali elevati e modelli non generalizzabili.

I modelli Euleriani-Lagrangiani tracciano le particelle individualmente risolvendo al contempo il flusso di gas su una mesh Euleriana. Uno di questi approcci è il Multi Phase Particle In Cell (MP-PIC), nel quale le particelle sono organizzate in gruppi definiti parcelle (o clouds) contenenti particelle con proprietà simili (massa, velocità, dimensioni) e le interazioni tra particelle sono rappresentate attraverso un modello degli sforzi che previene una compattazione irrealistica e simula statisticamente le dinamiche di collisione.

Sull'approccio MP-PIC si basa il software CPFD Barracuda utilizzato per la rappresentazione numerica degli esperimenti fatti ad IFPEN.

1.2 Obiettivi della Tesi

1.2.1 Revisione Sistematica della Letteratura

Il primo obiettivo è una revisione dello stato dell'arte con il doppio intento di:

- Stabilire lo stato di avanzamento della ricerca sull'argomento della simulazione di letti fluidizzati con una portata pulsante di gas in ingresso e determinare la curva di interesse generata dall'argomento nel tempo e chi sono i principali ricercatori dedicativisi.
- Recuperare importanti informazioni legate ai principali modelli numerici utilizzati per la rappresentazione di letti di particelle Geldart A, alle equazioni di chiusura scelte e ai principali parametri di simulazione.

1.2.2 Rappresentazione Numerica

Il secondo obiettivo è quello di preparare un modello computazionale capace di riprodurre i principali dati sperimentali ottenuti nell'impianto pilota di IFPEN, attraverso l'utilizzo del software CPFD Barracuda. L'intento è di ottenere un modello ben consolidato per la rappresentazione del fenomeno di fluidizzazione e di riprodurre l'impatto delle differenti frequenze di pulsazione applicate all'ingresso del fluido.

Una messa a punto dei parametri di simulazione e delle ipoTesi del modello per un progetto precedentemente sviluppato è effettuata. Il modello contiene già i file per la geometria e i dettagli della struttura, per la mesh e per le condizioni al contorno per un caso con portata di gas continua ma non prende in considerazione la possibilità di aggiungere una pulsazione al flusso in ingresso e nemmeno il trasferimento di massa, dunque non è presente l'Elio nella configurazione. In particolare, la messa a punto si concentra sul modello di drag, sulla frazione volumica di solido all'ingresso delle particelle e sui parametri di ritenzione del momento, di cui si parla in sezione 4.

Una volta perfezionato il modello per il caso in continuo, viene implementata la possibilità di aggiungere un flusso pulsante di gas e le frequenze di 1, 3, 5 e 7 Hz vi sono applicate per verificare l'adattamento dei risultati ai dati sperimentali.

1.3 Risultati

1.3.1 Revisione Sistematica della Letteratura

Una ricerca attenta sul sito web "Scopus" ha permesso di recuperare un totale di 126 articoli, di cui circa due terzi erano fuori tema, mentre la maggior parte dei restanti trattava solidi diversi dalle particelle Geldart A studiate in questo documento, concentrando l'attenzione su tre articoli.

Sono state ottenute interessanti informazioni riguardanti le equazioni di chiusura dei modelli utilizzati, sebbene tutti gli articoli modellassero con un CFD-TFM, e riguardanti i principali parametri di simulazione come il coefficiente di specularità (SC), il coefficiente di restituzione (RC) e il passo temporale. È emerso che una condizione di free slip alla parete è preferibile (significando un SC molto basso), che il RC è per la maggior parte imposto sopra

0.9 e che il passo temporale ha un'influenza importante sulle simulazioni CFD e deve essere scelto a un valore basso (solitamente tra 10^{-5} e 10^{-3}).

I principali risultati dei tre articoli sulle particelle Geldart A hanno mostrato che la pulsazione aumenta l'omogeneità del letto, la conversione dei reagenti e il controllo dell'agglomerazione. È riportato che frequenza, ampiezza e forma della pulsazione sono i parametri più influenti. In particolare, alcuni articoli hanno presentato frequenze elevate per aumentare la turbolenza nel letto, risultando quindi vantaggiose, mentre altri hanno trovato un maggiore controllo degli agglomerati a frequenze più basse.

Infine, gli ultimi articoli hanno evidenziato l'importanza della scelta del modello di trascinamento e hanno offerto un confronto tra i due diversi modelli, CFD e CPFD.

In conclusione, gli studi presenti in letteratura riguardanti letti fluidizzati pulsanti di particelle Geldart A sono ancora scarsi e sono stati trascurati a favore di letti meno problematici in termini di agglomerazione e fluidodinamica. I risultati trovati mostrano alcune discrepanze, ma sono, per la maggior parte, in accordo riguardo alla scelta dei parametri e alla necessità di adattare le equazioni di chiusura al caso specifico (tipo di solido e regime di fluidizzazione). Gli approcci Euleriano-Euleriano sono stati preferiti nella stragrande maggioranza degli articoli e pochissimi di essi hanno impiegato un approccio MP-PIC. Viene giustificata in questo modo la scelta di trattare la pulsazione nei letti di particelle Geldart A con il software CPFD.

1.3.2 Analisi di Sensibilità sul Caso in Continuo

Sono stati osservati tre parametri principali in questa analisi di sensibilità: il modello di trascinamento, la frazione volumetrica solida del flusso di particelle in ingresso e i parametri di ritenzione del momento (MRP).

È emerso che un modello di drag omogeneo è stato in grado di descrivere il sistema senza la necessità di una modifica della legge di trascinamento e, dati i risultati, la correlazione di Gidaspow sembra rappresentare meglio la fluidodinamica.

La frazione volumetrica solida ha avuto un impatto significativo, ma con una correlazione non ovvia ai risultati, che necessita di ulteriori approfondimenti. I valori tra 0.5 e 0.55 sembravano riprodurre la fluidodinamica osservata meglio del 0.4 di default del software, suggerendo un flusso più denso all'ingresso del reattore.

I parametri di ritenzione del momento hanno seguito il comportamento atteso e la condizione di "free slip" alla parete sembra essere quella che meglio riproduce le condizioni sperimentali. Infine, l'assetto di simulazione ottimizzato prevederebbe l'uso del modello di Gidaspow come modello di trascinamento, una frazione volumetrica solida compresa tra 0,5 e 0,55 e un MRP di 1. Gli effetti combinati di questi ultimi due parametri devono essere presi in considerazione.

1.3.3 Simulazioni con Pulsazione

L'impatto di quattro frequenze di ingresso del gas sulla fluidodinamica e sull'efficienza di stripping dell'elio è stato testato. In ultimo, il modello utilizzato comprendeva: Gidaspow come legge di drag, una frazione volumetrica del solido pari a 0.5 e un MRP pari a 0.2; diversa dalla configurazione ottimizzata in quanto, per limiti di tempo, si è dovuto cominciare lo studio sulle pulsazioni prima della fine dell'analisi di sensibilità.

I risultati relativi alla densità e all'altezza del letto hanno mostrato tendenze lontane da quelle sperimentali e un effetto complessivamente limitato della pulsazione del gas, mentre risultati migliori sono stati ottenuti per il calcolo dell'efficienza di stripping.

In conclusione, è necessario un ulteriore studio sull'argomento e l'utilizzo del modello ottimizzato derivante dallo studio alla sezione precedente dovrebbe essere utile per risolvere i problemi legati alla fluidodinamica. L'aumento del numero di frequenze simulate per corrispondere a quelle sperimentali e la rappresentazione della densità in funzione dell'altezza del letto potrebbero fornire indicazioni utili per la risoluzione dei problemi.

1.4 Conclusioni

Per riassumere, inizialmente è stata condotta una revisione sistematica della letteratura per analizzare i progressi e l'interesse della ricerca sull'argomento e recuperare informazioni importanti relative ai modelli e ai parametri di simulazione utilizzati per letti fluidizzati di particelle Geldart A con un ingresso pulsante. In secondo luogo, partendo dal lavoro già svolto presso IFPEN, uno stripper a letto fluidizzato su scala pilota è stato rappresentato numericamente utilizzando l'approccio MP-PIC per testarne la capacità di riprodurre i dati sperimentali.

Nella sezione 6, sono stati descritti il processo di ricerca e i suoi risultati. È stata riportata una scarsa quantità di studi, principalmente focalizzati su altri tipi di particelle che mostrano un comportamento di fluidizzazione migliore rispetto a quelle di tipo Geldart A. Gli articoli in revisione hanno mostrato un buon accordo riguardo alla scelta di modelli computazionali e parametri. Alla fine, la quasi totalità degli articoli ha utilizzato un approccio Euleriano-Euleriano con il Two Fluid Model, lasciando l'applicazione degli approcci Euleriano-Lagrangiani a letti di particelle aerabili come un campo con poca o nessuna letteratura e ancora da esplorare.

Nelle sezioni 7 e 8, è stato creato un modello CPFD del letto ed è stato condotto uno studio per la sua ottimizzazione e accuratezza rispetto ai dati sperimentali disponibili e sulla base delle informazioni ottenute dalla revisione della letteratura. Nella prima sezione, è stata eseguita un'analisi di sensibilità su tre dei parametri più influenti della simulazione: modello di drag, frazione volumetrica di solido in ingresso e parametri di ritenzione del momento. L'analisi ha mostrato che variando questi parametri era possibile ottenere una descrizione accurata della fluidodinamica del letto e un modello affidabile per una futura rappresentazione di diverse condizioni di flusso.

La rappresentazione della pulsazione ha mostrato risultati incoraggianti, in particolare per quanto riguarda l'aumento delle capacità di stripping dell'ingresso pulsante, che erano in accordo con gli esperimenti. Tuttavia, il modello non è riuscito a riprodurre le caratteristiche del flusso che non presentavano una grande differenza rispetto al caso continuo e mostrano tendenze piuttosto diverse rispetto a quelle sperimentali. L'uso di un modello non ottimizzato è attualmente il principale punto di migliorazione, ma un'analisi più approfondita dei risultati deve essere effettuata per avere una visione più chiara.

In conclusione, le simulazioni mostrano risultati incoraggianti, per questo motivo si suggerisce la prosecuzione del lavoro con l'approccio MP-PIC. Da una parte, si consiglia uno studio più esteso sull'impatto dei parametri di simulazione, come l'uso di due valori diversi per l'MRP o una maggiore attenzione ai coefficienti del tensore degli sforzi. D'altra parte, è necessaria una comprensione più approfondita della fisica e si raccomanda la prosecuzione degli esperimenti su scala di laboratorio e la ripetizione di questi esperimenti in diverse condizioni operative, come un flusso di solido maggiore all'interno dello stripper.

Questa prefazione inquadra dunque il lavoro di Tesi come un'investigazione tecnica e un contributo alla riduzione della distanza tra la ricerca sperimentale e la modellazione numerica di reattori a letto fluidizzato in condizioni di ingresso pulsato.

2 Abstract

This work investigates the simulation of pulsed fluidized beds using Computational Particle Fluid Dynamics (CPFD), applied to the stripping section of the Fluid Catalytic Cracking (FCC) process. Fluidized beds of Geldart A particles are widely used in FCC but face operational challenges such as particle agglomeration, bubble coalescence, and scale-up instabilities. Pulsed gas injection offers a promising process intensification method, improving gas-solid contact, mixing, and heat and mass transfer.

The study combines a systematic literature review with numerical simulations to assess the potential of CPFD for modelling pulsed beds. Out of 126 reviewed papers, only a small fraction focused on Geldart A particles with pulsed inlets. Experimental work has already been done at IFP Energies Nouvelles (IFPEN), which studied pulsed fluidization in a pilot-scale reactor by measuring bed bulk density, bed height, and mass transfer using a helium tracer.

Simulations were performed with the Barracuda CPFD software, which uses a hybrid Eulerian-Lagrangian MP-PIC approach. A sensitivity analysis on the continuous case evaluated the impact of drag models, inlet solid volume fraction, and particle-wall interaction parameters. The best agreement was provided by the Gidaspow model, momentum retention parameters both equal to one and a fraction comprised between 0.5 and 0.55. Pulsed inlet simulations at frequencies of 1–7 Hz reproduced experimental trends for the stripping efficiency of Helium, but further work is necessary to assess the hydrodynamics inside the vessel.

The results confirm the MP-PIC approach as an efficient tool for simulating such multiphase systems, paving the way for future integration of reaction kinetics and industrial-scale reactor modelling.

Contents

<u>1</u>	ABSTRACT	<u></u>
<u>2</u>	INTRODUCTION	11
2.1	1 FCC	11
2.2		14
2.2.	2.1 Process Intensification	15
2.2.		16
2.3	3 COMPARISON BETWEEN PULSED AND CONTINUOU	s Fluidization 17
2.3.	3.1 MINIMUM FLUIDIZATION VELOCITY AND PRESSU	RE DROP17
2.3.	3.2 Bubble Characteristics	18
2.3.	3.3 BED EXPANSION AND CLUSTER FORMATION	
2.3.	3.4 MIXING CAPABILITIES	19
2.3.	3.5 HEAT AND MASS TRANSFER	20
2.4	4 IFPEN's Previous Contributions	20
2.4.		21
2.5		24
2.5.		24
2.5.		
_	CINALLI ATION ADDDOACHES	27
<u>3</u>	SIMULATION APPROACHES	
3.1.	·	28
3.1.	1.2 Drag Models	29
3.1.	1.3 OTHER SIMULATION PARAMETERS	33
4	OBJECTIVES	
÷	<u></u>	
	4 B	27
4.1		
4.2	2 SIMULATION APPROACH	37
<u>5</u>	SYSTEMATIC LITERATURE REVIEW	
5.1	1 METHODOLOGY	39
5.2		40
5.2.		ion
5.2.		43
5.2.		45
J.J	CONCLUSIONS	43
_		
<u>6</u>	SENSITIVITY ANALYSIS ON CONTINUOUS CAS	SE 47
6.1	1 METHODOLOGY	47
6.2	2 SIMILI ATION SETUD	Δ7

6.2.	2.1 Starting Setup	47
6.2.	2.2 Modifications	49
6.2.	2.3 FINAL SIMULATION SETUP	50
6.3	RESULTS	50
6.3.	3.1 Drag Model	51
6.3.	3.2 SOLID VOLUME FRACTION	52
6.3.	3.3 MOMENTUM RETENTION PARAMETERS	54
6.4	CONCLUSION	56
<u>7</u>	PULSATED INLET SIMULATION	<u> 57</u>
7.1		
7.2		
7.3		
7.4	CONCLUSION	59
<u>8</u>	CONCLUSIONS	<u> 61</u>
8.1	L FUTURE PERSPECTIVES	61
<u>9</u>	BIBLIOGRAPHY	63
<u>10</u>	LIST OF FIGURES	<u> 66</u>
<u>11</u>	LIST OF TABLES	67

3 Introduction

3.1 FCC

Fluid Catalytic Cracking (FCC) is one of the most important gasoline-producing processes in the refinery.

From Figure 3.1 it is possible to see an overview of the refining process and the cuts going into the FCC. The process takes in the heavy gas oil coming from the atmospheric distillation column, in some cases combined with the residue from the atmospheric or the vacuum column (with a previous deasphaltation of the cut to avoid excessive coke formation), and converts it to a mixture of C_5 - C_{11} alkanes and alkenes, and aromatics, with a relatively high octane number (RON 90-94) [1]. These products are then included in the gasoline pool, allowing a greater yield and quality of gasoline from the crude oil.

From Figure 3.2 it is possible to see a scheme of the reactor paired with the catalyst regenerator. The feed is pre-heated and then sent to the riser section of the reactor. The reaction occurs almost entirely inside the riser, where the hot regenerated catalyst $(677 - 732 \, ^{\circ}\text{C})$ immediately vaporizes the feed, bringing it to working temperature $(496 - 565 \, ^{\circ}\text{C})$ [2].

Exiting the riser, the catalyst is conveyed to the reactor vessel where the presence of cyclones and/or disengaging devices allows to separate it from the volatile reaction products and redirecting it towards the stripping section, where counter-current steam is used to strip the last compounds trapped inside the catalyst pores to avoid further reactions. The solid is accumulated at the base of the vessel, partially blocked by either a slide or a plug valve, to stop volatile flammable compounds from accessing the regenerator section.

The cracking reaction leaves a residue of coke on the catalyst that deactivates it, therefore a regeneration is needed and it is achieved through combustion of said coke in presence of combustion air and at high temperatures that can vary from 640°C to 730°C [2], based on the working condition chosen (low, intermediate or high regeneration). Furtherly, the heat of regeneration brought in the reaction through the catalyst powder, that works as an energy vector, will not only vaporize and bring to the desired temperature the feed but also help compensate the heat loss due to the endothermic reactions.

Finally, the flue gases from the regenerator section are going to pass through a cyclone, to avoid any solid residuals, and then undergo energetic valorisation and waste treatment.



Basic Refining Concepts

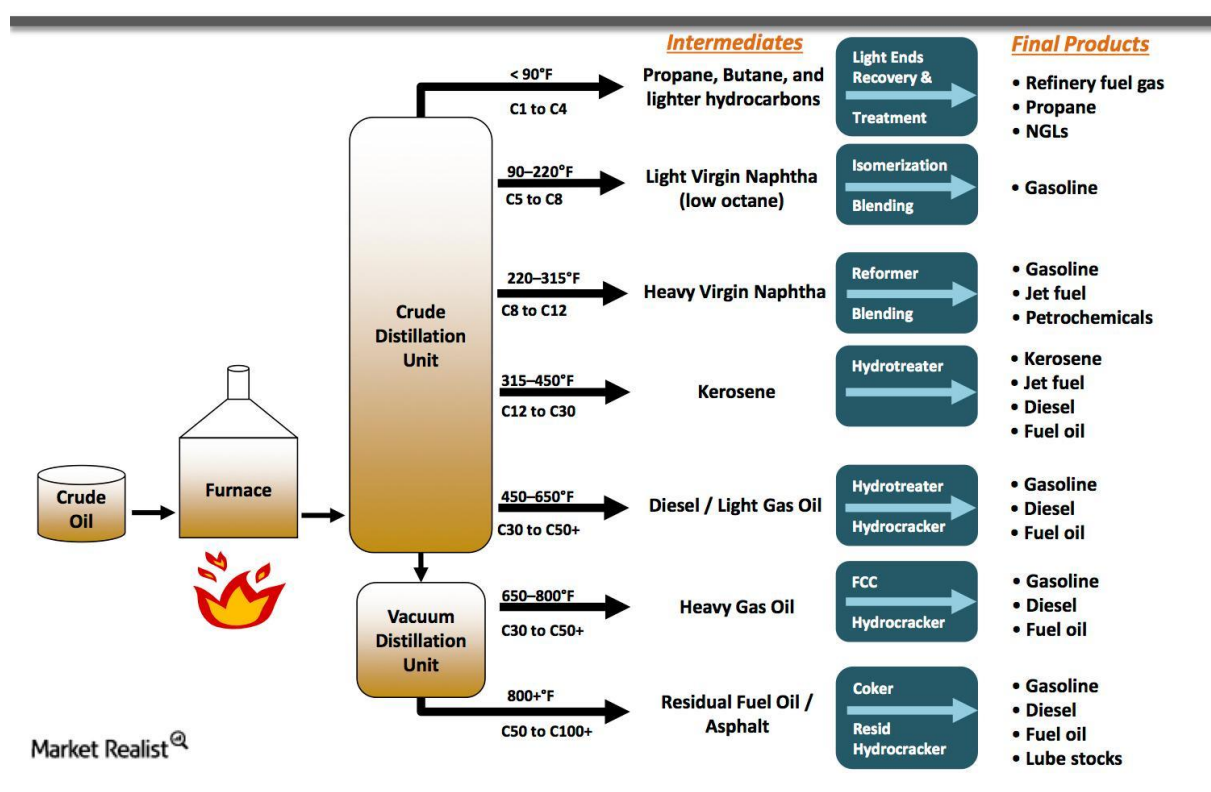


Figure 3.1: Refining process cuts and final products [3]

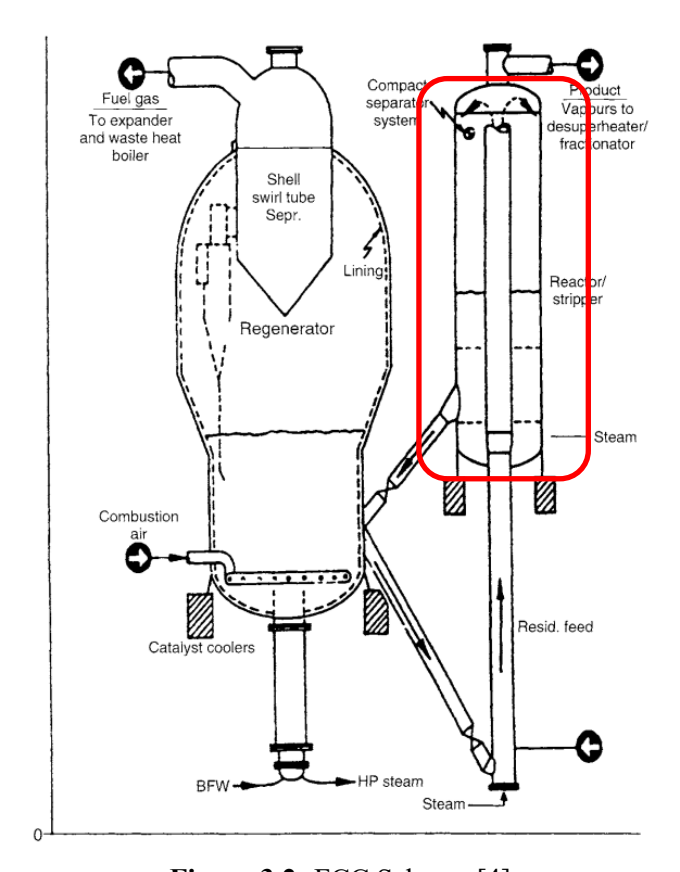


Figure 3.2: FCC Scheme [4]

REACTION AND CATALYST

The main reaction is a scission of the carbon-to-carbon bonds through the acid-catalysed formation of carbocations that undergo numerous rearrangements. The process leads to the formation of straight and branched-chain alkanes, branched alkenes (olefins) and cycloalkanes (naphthenes). A furthering of the reactions leads instead to even smaller alkenes and branched alkenes, simple aromatic compounds in the gasoline boiling range and carbon coke which, as afore mentioned, is deposited on the catalyser surface.

The catalyst is typically composed from 20 to 40 % in ultra stable Y Zeolite included in a matrix of amorphous silica alumina, a binder and a series of different possible additives, all having a great impact on the yield, coke make and product quality [1], as illustrated in Figure 3.3. Its bulk density usually spans between 0.80 to 0.96 g/cm³, with particle size distribution from 10 to 150 μ m and an average particle size of 60 to 100 μ m [5], placing the catalyst in group A of the Geldart classification for fluidization, as shown in Figure 3.4.

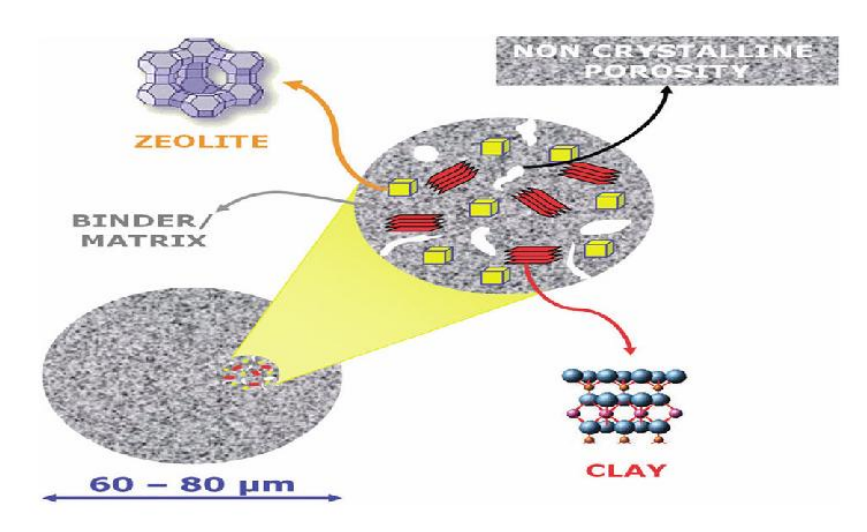


Figure 3.3: FCC catalyst [6]

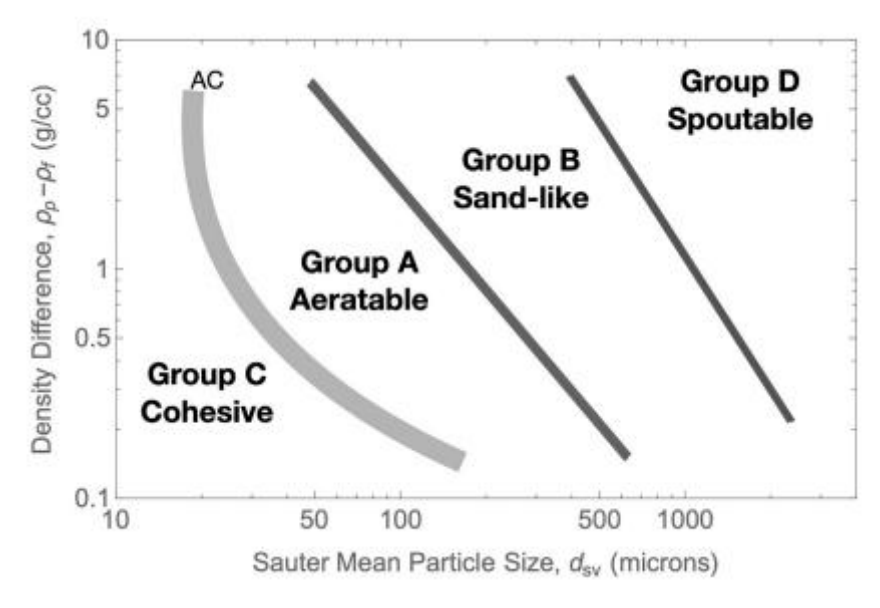


Figure 3.4 : Geldart Classification [7]

3.2 Fluidized Beds

In this project, the focus is posed on the stripping part of the FCC process, represented in the red square of Figure 3.2, and in particular on the hydrodynamics inside the vessel, which is in fact a fluidized bed of Geldart A particles.

Fluidized bed reactors are defined as heterogeneous reactors in which the solid particles (frequently with a diameter of less than 0.1mm) behave like a fluid due to the circulation of a gas or liquid flow sent through a sparger, usually at the bottom vessel. One of its main advantages is therefore an extremely efficient contact between the solid and the fluid, leading to enhanced heat and mass transfer as well as reaction rates and allowing for an ideal control of the temperature, making it the perfect reactor for highly exothermic reactions or ones where the product may go through thermal degradation. [8]

Despite the well diffused application, this technology still presents problems related to many aspects of its operability and scale-up. Not all solids have the same response to fluidization, which varies based on their composition and dimensions. Coarser particles may have trouble to be suspended, while finer particles present problems of agglomeration or cluster formation due to interparticle cohesive forces. For the most, the effects of these forces on the flow change drastically based on the scale of the unit, which contributed to a vision of the fluidized bed as an instable system, where the smallest external interference can create a change in hydrodynamics. [9]

In Figure 3.5, the qualitative representation of the fluidization states for a Geldart A powder is presented, with the increase of gas velocity from left to the right side of the image. Initially, the powders are in a condition of packed bed, for which the gas drag force is not sufficient to expand or fluidize the bed of powders. Then, at the minimum fluidization velocity, the powder starts to be fluidized, which is represented by an increased gas drag force that is sufficient to support the bed weight and increase the distance between the particles in the bed (bed expansion) and create recirculation patterns that improve the heat and mass transfer. This region is defined as homogeneous or smooth fluidization and it is attributed to fluid-solid or solid-solid interactions, with particle clustering playing an important role in the developing of this hydrodynamics. Contrarily to other types of powders, the formation of bubbles inside the bed does not happen at the reaching of the minimum fluidization velocity, but at a higher one, called minimum bubbling velocity. Once this velocity is reached, the bed enters the bubbling regime, characterized by small bubbles that increase in dimensions as they rise, due to the lower permeability of these powders that encourages coalescence. As the velocity increases, coalescence becomes more and more important, with bubbles arriving at the same diameter of the vessel and acting like pistons of gas on the particles; this phenomenon is called slugging. Finally, the more the velocity is increased the greater the turbulence inside the bed is, leading to the formation of a turbulent regime with possible entrainment of solids.

In certain cases, a high velocity gas current can be used for the transportation of particles from one vessel to another. This is very common in the food or pharmaceutical industry, where there might be the need to move small powders without human intervention, avoiding in this way possible contamination.

Geldart A particles show a relatively high heat and mass transfer when fluidized, making them ideal for fast, exothermic or endothermic reactions [7].

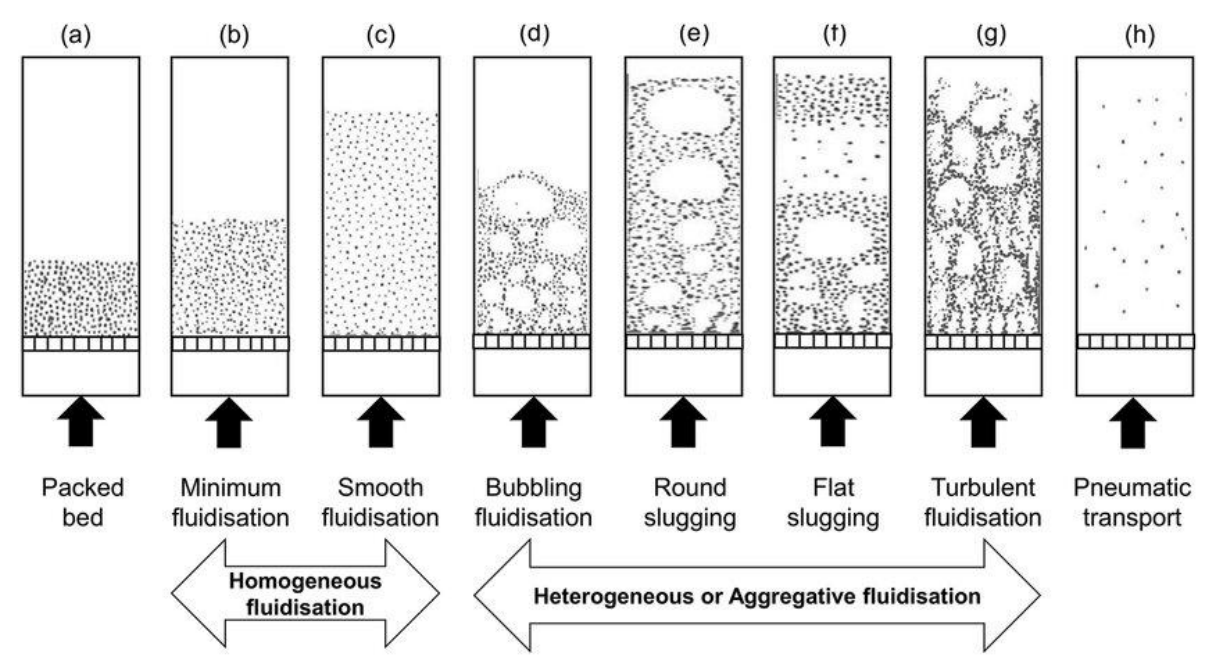


Figure 3.5: Different regimes of fluidization for a fluidized bed [10]

3.2.1 Process Intensification

To improve the performances of these types of reactors, it is then necessary to reduce particle agglomeration and avoid the formation of preferential pathways for the gas or bubbles of big dimensions, in a way to increase the contact between the fluid and the solid, the mass and heat transfer coefficients, and therefore to favour the reaction; it is also important to act on the reproducibility of the flow hydrodynamics to be able to have a more controlled and predictable structure, simplifying the scale-up and the development of systematic approaches. The strategies operated for the resolution of these problems are divided in three, namely by acting on the particle-particle contact forces, on the body volume forces or on the particlefluid surface forces. The first strategy involves either the use of conditioners like liquid binders or flow-conditioning particles either the modification of the working conditions, like a change in temperature or pressure or even working under supercritical conditions; they clearly represent more ad hoc solutions rather than universal designs. The second strategy aims to obtain the so called "high-gravity fluidized beds" by altering the gravitational pull on the particles through the use of vortex gas flow to control the solid volume fraction inside the vessel. Electrical or electro-magnetic stabilization are also viable options to stabilize the bed, although, not as diffused due to the imposition of a rigid meso structure, which results in a reduction of the transport and transfer coefficients [9].

About the third strategy, various and different options have been identified to obtain what has been defined as a "structured fluidized bed":

- Some of these introduce geometrical constraints on the particles, acting on polydispersity, shape or roughness. In particular, polydisperse groups of particles, made up of coarser and finer solids can reduce the formation of clusters and improve the flowability, even though their impact is often difficult to predict.
- Some pose constraints on the flow with the use of internals such as baffles or distribution plates which allow to break the growth of bubbles and avoid the formation of preferential paths, but that represent a sort of a trade off between better gas-solid contact (and gas hold up) and higher pressure losses in the column. Although very effective, they are intrusive and, oftentimes, fixed solutions that remain case-specific,

- and same goes for the setting up of multiple injection points, which has obvious impact on the distribution of the gas in the vessel and consequently a reduction in dimensions of the bubbles.
- Finally, some pose dynamical constraints either on the particles (vibration through the use of high intensity, low frequency sound waves) either on the flow, through the use of a pulsating fluid flow. These are the most popular due to their non-intrusive character and simplicity.

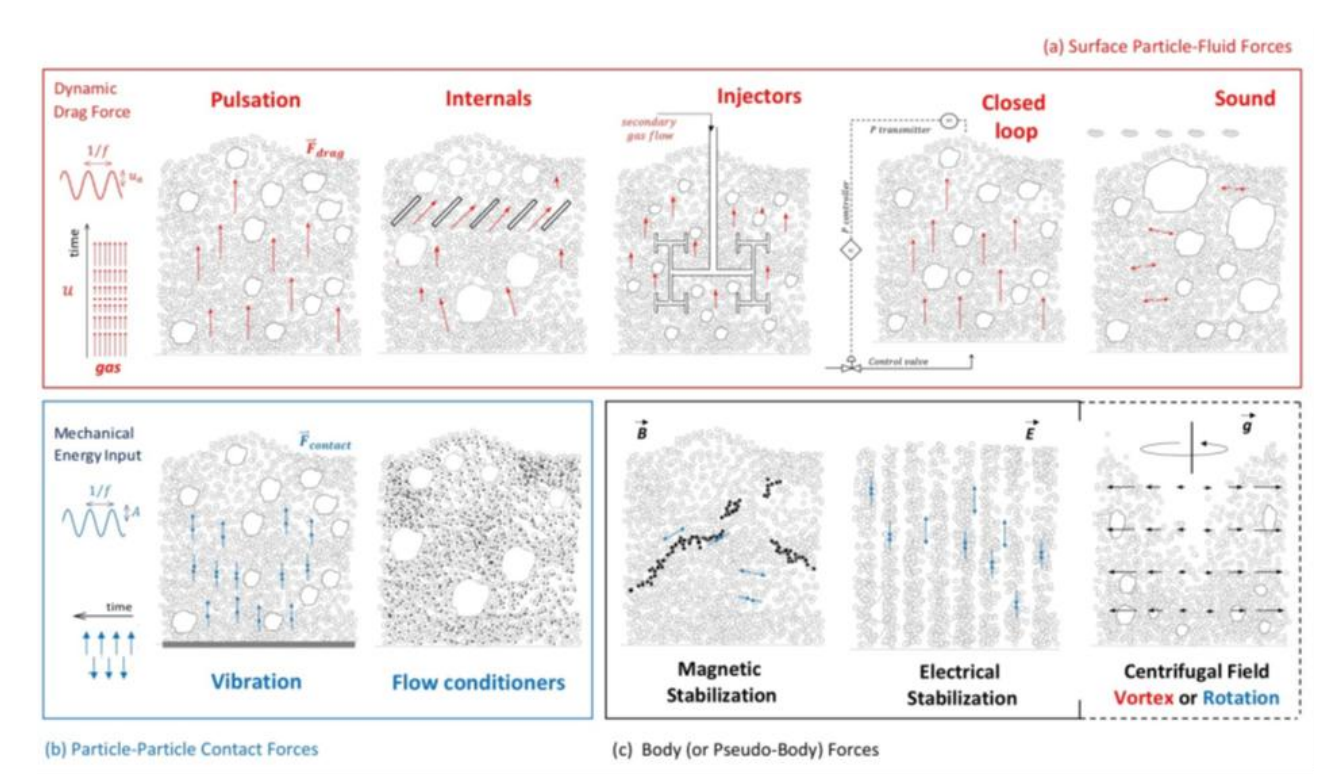


Figure 3.6: Process intensification methods for fluidized beds [9]

3.2.2 Gas Pulsation

The use of a pulsating flow has been studied since the 1960s but has been limited in the industrial applications due to multiple factors such as a slow renovation rate in the machinery because of the long lifespan of the components, difference in behaviour based on type of solid and a relationship between frequence and fluidization behaviour which is still under study. The most common pulsation functions are the sinusoidal and the square one, while the sawtooth and rectangular ones are less used; all with frequencies on the 0-15 Hz range [11]. It is possible to distinguish between two main families of pulsation devices: relocating and intermittent. A relocating flow is characterized by a continuous gas flow that is relocated in different parts of the bed through a rotating disc with an open area. Intermittent flow is instead characterized by an "on" and a "off" phase causing the pulsation effect. This has two impacts that differ greatly from the relocating device: a bigger pressure build up on the back of the valve, which causes more important mechanical stresses, and the occurring of defluidization of the bed during the "off" phase, which has been often attenuated via the use of a second pulsation device in concurrence with the first valve. Solenoid valves have largely been used for this application, but have found success mostly at laboratory scales because of

the increased time related to the mechanical constraints given by the bigger inertia of the armature [12].

Follows, in the next section, a review of a series of the most common fluidization behaviour indicators to make a point of the differences and advantages brought by the pulsating bed in comparison with the continuous one.

3.3 Comparison between Pulsed and Continuous Fluidization

3.3.1 Minimum Fluidization Velocity and Pressure Drop

The minimum fluidization velocity is defined as the superficial fluid velocity at which the fluid drag force balances the gravity acting on the bed, and it is often calculated through a correlation based on the Ergun equation:

$$(1 - \varepsilon_{mf}) \left(\rho_s - \rho_g\right) g = 150 \frac{\left(1 - \varepsilon_{mf}\right)^2}{\varepsilon_{mf}^3} \frac{\mu v_{0mf}}{D_p^2} + \frac{7}{4} \frac{\rho v_{0mf}^2}{D_p} \frac{\left(1 - \varepsilon_{mf}\right)}{\varepsilon_{mf}^3}$$
 (1)

Where ε_{mf} is the void fraction of the bed at minimum fluidization, ρ is the density of solid (s) and gas (g), g is the acceleration of gravity, μ is the fluid viscosity, v_{0mf} is the minimum fluidization velocity, and D_p is the particles diameter.

Often, in literature, a graph of the pressure drop in function of the superficial fluid velocity is used, like the one in Figure 3.7, instead of simply the minimum fluidization velocity. Usually, for small Reynolds value, the curve shows a linear growth up until the point where the bed becomes fluidized; at the point of minimum fluidization the curve flattens out until a plateau value, which is where entrainment of the solid starts.

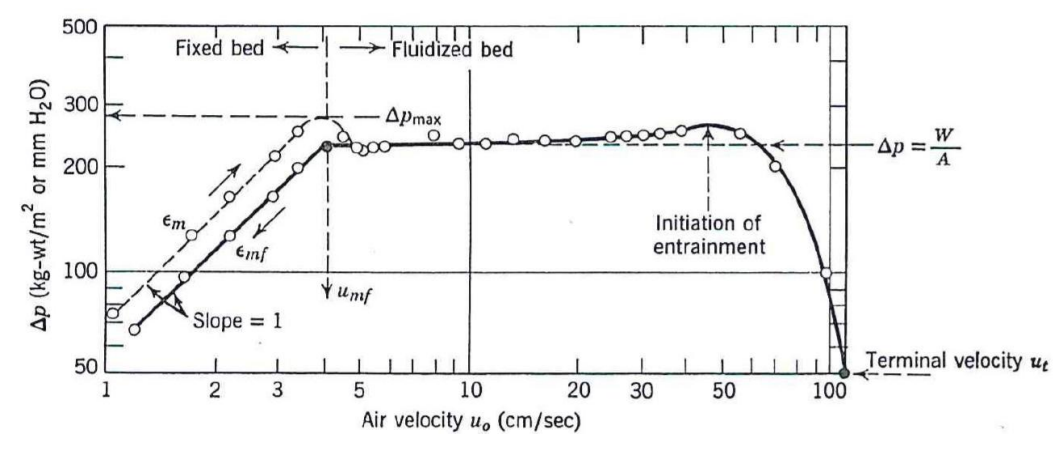


Figure 3.7: Pressure drop behaviour in fluidized beds [13]

For what concerns pulsed fluidized beds, many papers in literature report a smaller minimum fluidization velocity if compared with the continuous case. Bizhaem & Tabrizi [14] studied a bed of silica particles, classified as on the Geldart A/B border, with a pulsation frequency of 10 Hz, finding a reduction up to a third of the velocity required for the continuous case, passing for instance from 2.1 cm/s to 0.7 cm/s. Many studies have also found a smaller velocity for higher frequencies in the range 0-15 Hz, related to a reduction of the pressure drop [14]. In general, pulsed flow potentially reduces up to 76% the minimum fluidization velocity necessary [11].

Finally, Nishimura et al. [15], while studying Geldart A and B particles, found that more cohesive particles (in a 0.2-1 Hz range) presented minimum fluidization at bigger fluid velocities if compared with the continuous conditions, showing a dependency of the trend on the particle characteristics.

3.3.2 Bubble Characteristics

Bubbles are constituted by a particle free void, filled with gas; they represent a zone of no contact with the solid, therefore reducing the performance of the bed, but at the same time they increase its mixing capabilities due to the increased movement of the solid in the vessel. Because of this, they have often been used as a tool to analyse the impact of certain techniques or parameters on the fluidized bed reactors.

Wong & Baird found out that pulsation decreases the dimension of bubbles in Geldart B particles, while Bizhaem & Tabrizi [14] related the increase of frequency with a reduction of the bubble dimension. This has been explained as due to the air let in during the "on" phase, and particularly it has been found that bubbles are bigger for frequencies of 1 Hz if compared with the ones at 4 and 10 Hz, which are progressively smaller, because of the bigger "on" time of the fluid flow. Bubbles at 10 Hz and in the middle of the column were also found to have the same dimensions as the ones caused by a continuous flow, but the ones above the middle section were still smaller; this was due, explained the authors, to a lower tendency to coalesce of the bubbles in a pulsed flow.

So, pulsed flows appear to lead to better contact between gas and solid thanks to the reduction in size of the bubbles and the obstruction of their coalesce along the column, while the frequency of pulsation has an impact on the amount of this reduction, favouring smaller dimensions at higher frequencies.

3.3.3 Bed Expansion and Cluster Formation

Bed expansion is related to interparticle and particle-fluid interactions, it is measured at the top surface of the bed and the measurement results oftentimes complex as the bursting of bubbles at the top might be misleading.

Koksal & Vural [16] found that, at the lower range of 1-10 Hz frequencies tested, the bed expansion was lower than for a continuous flow, while at higher frequencies it was comparable even if with more homogeneous and smoother bed behaviour. Zhang & Koksal [17] then found that the bed shows an oscillation related to the respective frequency applied and that for smaller ones a bigger amplitude was observed. The authors concluded that the greater amplitude of the oscillation was the result of longer "on" period that were leading to bigger bubbles and therefore bigger bursts at the surface of the bed.

The greater homogeneity of the bed is beneficial also to counteract another phenomenon, the clustering of particles. The phenomenon is mostly related to the solid characteristics like size and density, but also to its moisture content. Again Zhang & Koksal [17] found that agglomerates would resent of the frequency of the pulsation by being forced in greater displacements and being more susceptible to breakage, especially at lower frequencies due to a greater amplitude of oscillation of the bed (Figure 3.8).

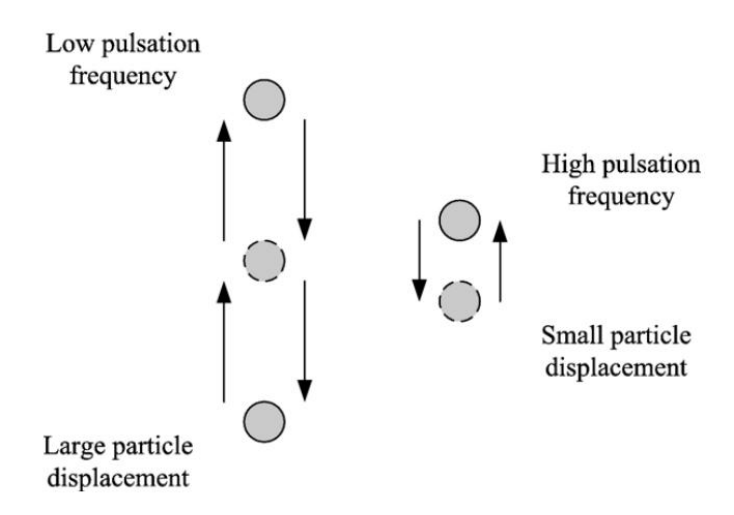


Figure 3.8: Particle displacement in function of pulsation frequency [17]

3.3.4 Mixing Capabilities

Many studies have suggested a great improvement in mixing times for pulsating fluidized beds, despite a great use of qualitative methods instead of quantitative ones.

For example, Hadi et al. [18] investigated a bed of Geldart A/B border particles with a wide size distribution and with the smaller size particles causing agglomeration. They studied the effect of pulsation on the mixing of the bed by colouring 40% of the particles and observing mixing over a time series. Using the same superficial velocity, it took only 3 seconds to mix in the pulsed fluidization regime, while it took 10s in the continuous one. The same method was used by Akhavan et al. [19] that used Geldart B particles instead. They noticed a reduction of the lifespan of agglomerates, validating other studies reported earlier in this document, and found similar results to the ones of Hadi et al., demonstrating the improvement in mixing coming from pulsating regimes.

A qualitative example of the increased mixing performance of pulsation is shown in Figure 3.9.

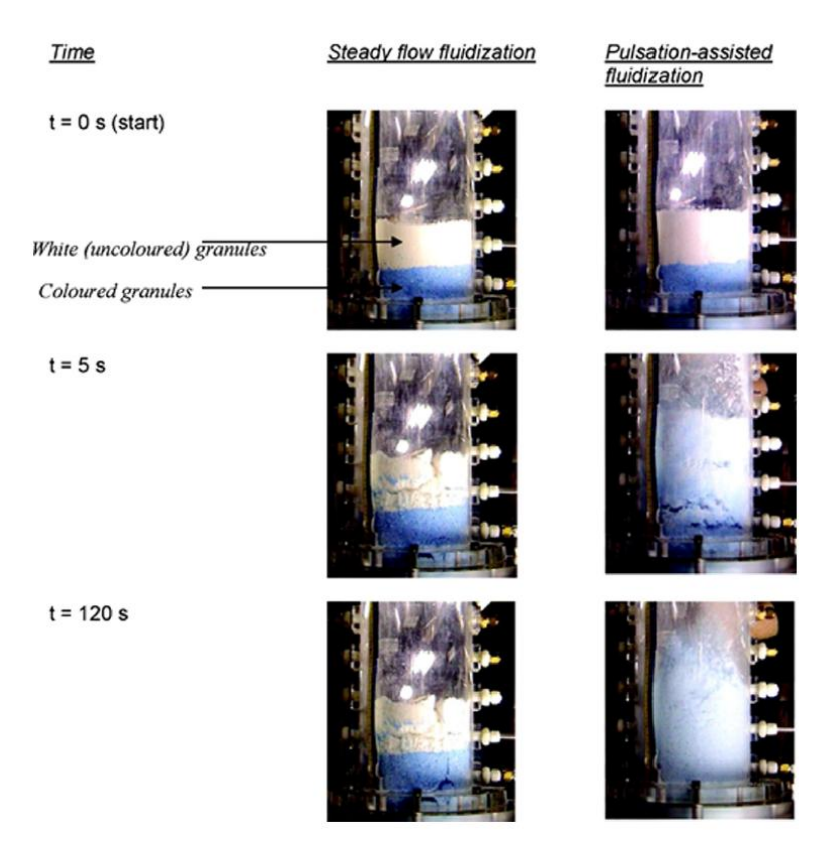


Figure 3.9: qualitative analysis of mixing performance of wet Geldart B particles: Continuous flow vs 3Hz flow [19]

3.3.5 Heat and Mass Transfer

Heat and mass transfer are also highly impacted due to the improved mixing, the higher bed homogeneity, smaller bubbles and therefore better gas-solid contact, and pressure drops that lead to a shorter agglomerate lifespan in the vessel.

Not many studies have been conducted on mass transfer and among these we find the one of Reyes et al. [20] that focused on the use of a combination of microwaves and pulsation on a drying unit for turnip seeds and that succeeded in increasing the effective diffusivity by four times, if compared to a continuous flow.

Most of the studies focused on heat transfer. For example, Zhang & Koksal [17] found that heat transfer was increased by 17-33% in group B particles with a pulsation of 7-10 Hz. Jezowska [21] found uniform temperature distributions inside the bed, indicating a more homogeneous heat transfer.

3.4 IFPEN's Previous Contributions

Pulsation therefore presents itself as a great opportunity to increase the efficiency of fluidized beds and improve their controllability and scalability and has been receiving increasing attention from the scientific community. Among them, IFP Energies Nouvelles was able to recognize the major energy saving possibilities of this technique, in line with the most recent efforts in terms of environmental impact, and started working on a pilot scale fluidized bed, retrieving further experimental evidence on the matter.

The aim of their experimental work was to evaluate the effect of pulsation on the fluid dynamic and on the mass transfer inside a circulating fluidized bed, testing in a range of

frequencies of pulsation going from 1 to 7 Hz. In particular, the mass transfer has been evaluated through the injection of Helium gas at the top of the stripping unit, together with the solid particles, and its concentrations taken at the exit of the vessel. Further measurements included the pressure drops across different sections, to calculate the bed density and bed height, and the bubble dimensions.

The catalyst's physical properties and particle size distribution (PSD) are reported in Table 1, while the air and Helium properties can be found in Table 2.

Table 1: Properties and PSD of the catalyst particles.

Solid Properties

Close pack volume fraction	0.63
Density (Kg/m3)	1500
Sauter Diameter (µm)	66
Initial bed height (mm)	735
Initial bed volume fraction	0.479

PSD

Size [µm]	Fraction
187	0.0165
143	0.0855
109.3	0.1762
83.6	0.2391
63.9	0.2241
48.8	0.1582
37.3	0.0758
28.5	0.0246

Table 2: Properties of the air at the injector and of the Helium at the solid inlet.

Air Properties

Density ρ (Kg/m ³)	1.29
Dynamic Viscosity μ (Kg/m/s)	1.79*10 ⁻⁵
Superficial air velocity v ₀ (m/s)	0.1
Normal Flowrate Qair (Nm³/h)	1.8

Helium Properties

Density ρ (Kg/m³)	0.187
Normal Flowrate Q _{He} (Nm ³ /h)	0.05

3.4.1 Pilot Scale Reactor

A sketch of the unit is reported in Figure 4.10. This configuration is a circulating fluidized bed whose main components are a fluidized bed stripper C-01, a solid riser R-01 and a cyclone separation unit V-01. Other important units are the solid inventory storage tank T-01 and the filter Y-01 for gas solid separation of the air leaving the unit.

The solid is introduced inside the riser, a vertical column 3 meters high and with 8 cm diameter, and a large gas flowrate carries it upward inside the cyclone, where gas solid separation occurs. In particular, the gas velocity inside the riser corresponds to 3.77 m/s, that means 60 Nm³/h, and to 13.56 m/s in the cyclone inlet. The gas leaves the cyclone and goes inside a filter before being released in the atmosphere, and the solid flows down the cyclone dipleg inside the stripper unit.

The stripper is an 80 mm diameter per 1.2 m high cylindrical vessel, that is represented in Figures 4.11. The air flowrate is provided from the bottom of the unit, in counter current to the solid, through a distributor whose geometry is reported in Figure 4.12. The gas and a small amount of entrained solid leave the unit from the top outlet and go back to the storage tank, while the solid flows down inside the standpipe previously described. The gas flowrate in the stripper can be provided in continuous or pulsed conditions through a system composed of a butterfly valve, to control the gas flowrate in the stripper, and a solenoid valve to create pulsation.

Different pressure drops measures are taken around the unit: one measure is taken across the riser, named PDT120, other two inside the fluidized bed, named PDT130 and PDT 140. PDT130 is used to evaluate the bed height; one extremity is found 60 mm above the gas distributor and the other one 760 mm above it. PDT140 shares the same lower extremity but has the second one at 260 mm from the distributor, and it is used to evaluate the bed density. These measures can easily be seen in the sketch reported in figure 4.11.

The unit operates at ambient temperature conditions, without reactions occurring, and at atmospheric pressure at all the gas outlets, although, some small differences in pressure measures are found, due to the solid flowing.

The geometric characteristics of the stripper are resumed in Table 3.

Table 3: Stripper's geometric characteristics.

Stripper's Geometric Characteristics

Vessel D (m)	0.08
Vessel H (m)	1.2
Dipleg length (m)	0.684
Dipleg D (m)	0.04
Top outlet D (m)	0.04
Bottom outlet D (m)	0.04
Outlets length (m)	0.15
Central tube sparger D (m)	0.0137
Lateral tubes sparger D (m)	0.008
Sparger holes D (m)	0.0015
Sparger holes number	10.5

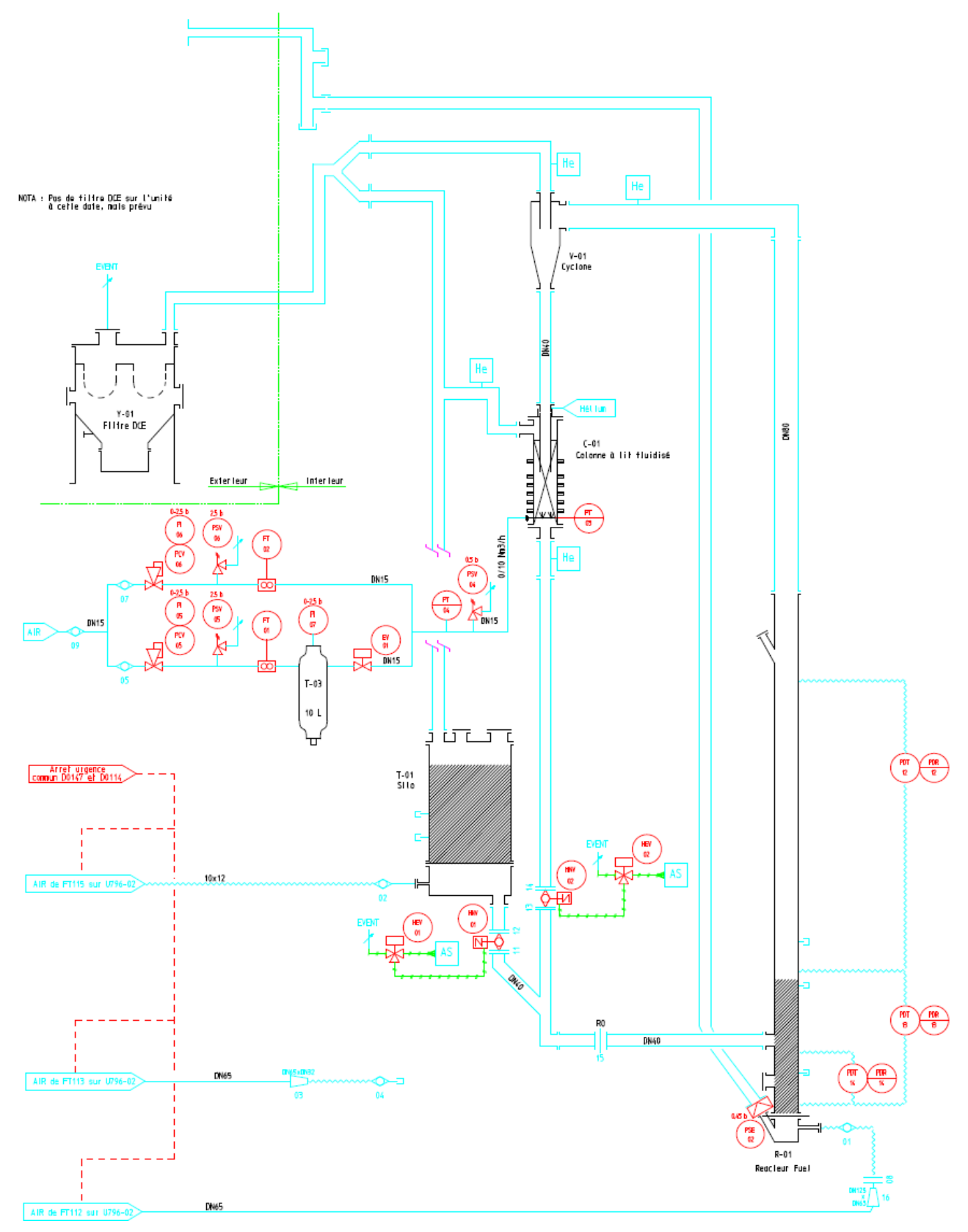


Figure 3.10: P&ID of the circulating fluidized bed

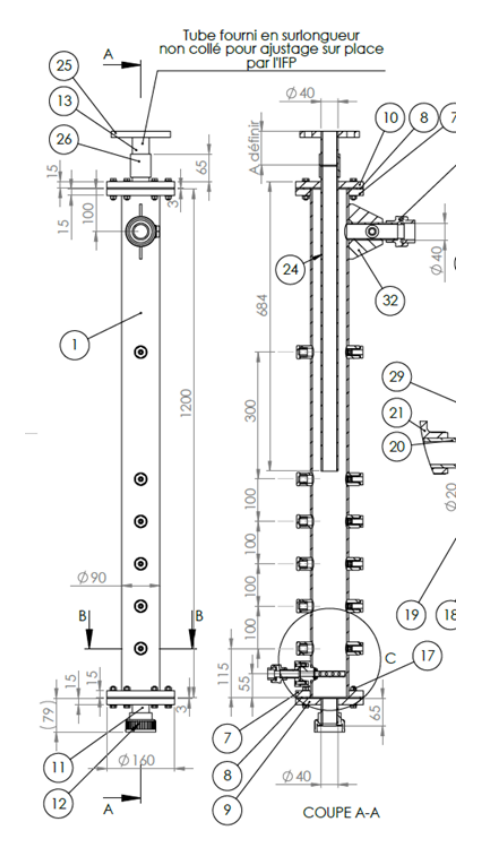


Figure 3.11: Gas sparger with dimensions

Figure 3.12: lateral and frontal view of the stripper

3.5 Main Experimental Results

In this section, the main experimental results coming from the pilot scale work of IFPEN, of interest in the context of the validation of the CPFD model, have been selected and resumed.

3.5.1 Bed Density and Bed Height

The pressure drop measurements PDT130 and PDT140 allow to assess bed height and bed density. These values are interesting because they characterize the fluidized bed, and they can be easily compared to numerical simulations to check if the model used correctly describes the physics of the system. Since in a fluidized bed, for the momentum balance, the pressure variation across a certain height is equal to the product of bed density, height and gravitational acceleration, the evaluation of density and height is based on the equation:

$$\Delta P = \rho \cdot \varepsilon_s \cdot g \cdot \Delta h \tag{2}$$

PDT140 can be used to assess the bed density ($\rho \cdot \epsilon_s$), since the distance between the measuring points is fixed at 20 cm. And once this value is known, with the assumption of constant bed density in the vertical direction, an estimation of the bed height can be done from the value of PDT130. This assumption is quite strong, since in this kind of bed with a dipleg in the middle, and therefore a reduced surface area at the top of the unit, a big coalescence of bubbles towards the top has often been observed. This probably causes a reduction in bed density at the top, and consequently an increase of the height compared to the calculated values.

Table 4: **Bed density at different frequencies for a solid flux of 15 kg/m2/s.** reports the different calculated densities at the various frequencies while in Table 5 we can find the bed heights. All these values are evaluated at 15 kg/m²/s.

Table 4: Bed density at different frequencies for a solid flux of 15 kg/m²/s.

Pulsation	Average PDT140 (mbar)	ε (-)	Bed Density (Kg/m ³)
Continuous	14.087	0.4786	718.668
1 Hz	12.386	0.4208	632.090
2 Hz	12.344	0.4194	629.907
3 Hz	12.161	0.4132	620.624
4 Hz	12.311	0.4183	628.266
5 Hz	12.448	0.4229	635.237
6 Hz	12.972	0.4407	661.887
7 Hz	13.176	0.4477	672.295

In all the pulsed tests the pressure drop measured is smaller if compared to the continuous case, although at high pulsation frequencies it increases again, getting closer to the continuous case values. Huge bubbles have been observed at the bottom of the column at low pulsation frequencies, meaning that a lot of air is present at the bottom, and it is therefore expected to have a low bed density.

Table 5: Bed height at different frequencies for a solid flux of 15 kg/m²/s.

Pulsation	Average PDT130 (mbar)	Bed Height (m)
Continuous	43.6870	0.7347
1 Hz	39.3176	0.7491
2 Hz	39.3861	0.7524
3 Hz	38.1190	0.7411
4 Hz	37.6235	0.7254
5 Hz	40.0639	0.7579

3.5.2 Helium Tracer Experiment

The results related to three different tests at a solid flux of 15.15 kg/m²/s and three at 32 Kg/m²/s are reported. The average values and the normalized ones of Helium fraction at the top exit of the stripper are reported in Table 6, for the 15.15 kg/m²/s case. The normalized values are evaluated as the ratio of He fraction at the top of the stripper for each pulsation over the He fraction obtained in continuous operations. The data for the 32 Kg/m²/s are directly reported in Figure 3.13.

Table 6: Helium fraction at the top exit of the stripper.

	Average (PPM)	Normalized
Continuous	794.2982	1
1Hz	1044.875	1.3155
3Hz	948.7971	1.1945

5Hz	989.3252	1.2455
7Hz	894.9988	1.1268

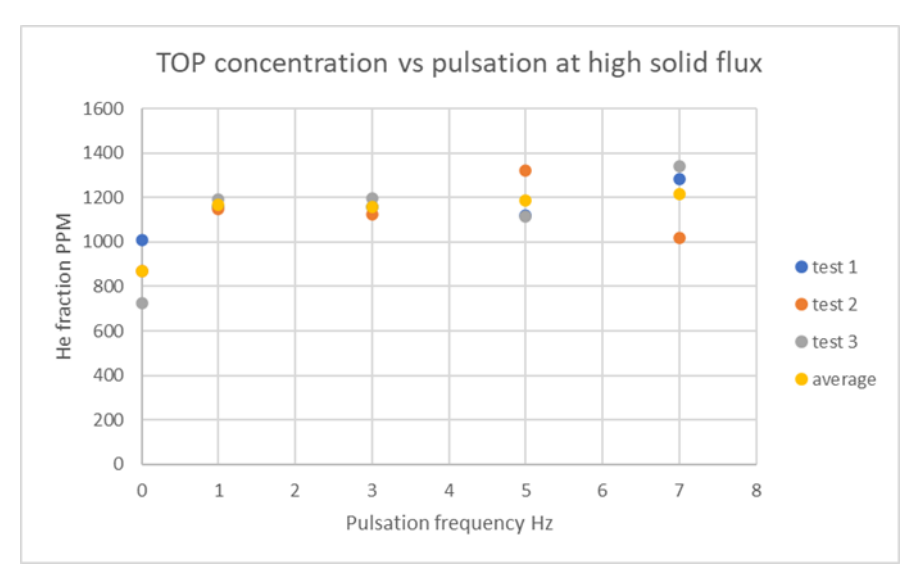


Figure 3.13: results of He tests with average values at $32 \text{ kg/m}^2/\text{s}$

4 Simulation Approaches

CFD representation of monophasic systems is nowadays a common and well understood practice, although the difficulties increase noticeably when dealing with multiphase systems and, in particular, the ones with presence of one or more particulate phases. The interactions between particles and between fluid and particles represent the biggest challenge.

The most accurate method is the Direct Numerical Simulation (DNS) which resolves the flow field on a scale smaller than the particle dimension and therefore requires no further modelling of interphase interactions [22]. For the same reason, it is also the most expensive from a computational point of view and it is mostly used only for the modification and fitting of certain models to specific cases of interest. Apart from the Direct Numerical Simulation (DNS), the simulation approaches can be divided into two big families: the Eulerian-Eulerian or CFD approach and the Eulerian-Lagrangian or Discrete Particle Model (DPM) approach.

The Eulerian-Eulerian approach is represented by the Two Fluid Model (TFM) which treats the two phases as interpenetrating continua on a macro-scale and calculates the pseudo-fluid rheological properties of the particles, like solid viscosity or granular temperature, through the Kinetic Theory of Granular Flow (KTGF) [23]. Attempts at using a coarser grid with this type of model gave acceptable results for the bigger particles of the groups B or D, although many papers reported various imprecisions in the representation of beds of finer solids, especially with the Geldart A particles, due to the presence of important interparticle cohesive forces, comparable to the gravitational ones. Neglecting these forces means implicitly assuming that the collision forces have the main role in the dissipation of the dynamic energy of the single particles, thus leaving the remaining part of energy for their propulsion towards the top of the vessel, which has lead in certain cases to an over-prediction of as much as 100% of the bed expansion [24]. Deen et al. [25] also reported that the TFM might over-estimate mixing because of the omission of solid friction in the KTGF. Furthermore, another drawback in the TFM is the difficulty in representing a solid phase with a distribution of different sizes; in fact, a phase with a PSD is usually reproduced by defining a different phase for each particle diameter, or by a Population Balance Model. However, the resolution of the mass and momentum equations for each phase or the Population Balance equation find a limited application due to their high computational cost [26].

An alternative to the TFM comes from the DPMs. Here the scale is smaller than in the Eulerian-Eulerian solution but still larger than the particle's diameter, meaning that the exchange of forces between fluid and solid cannot be computed by an integration on the particle's surface. A method using this approach is the Multiphase Particle in Cell (MP-PIC), in which the particles are organized in parcels, each containing a certain number of them, all with identical velocity, density and volume; a Liouville equation for particle distribution controls the evolution of the particle phase, resulting in a computational technique that can handle different particle size and types. The main difference with the TFM is that it models particle-particle interactions with the solid stress tensor equation instead of the KTGF and it also uses a simpler equation for the solid stress, without taking into account the shear stresses [27]. The solid stress, which is usually difficult to describe for particles in dense phases, is calculated as a gradient on the grid and then interpolated to the discrete particles [28].

Based on the MP-PIC approach is the Computational Particle Fluid Dynamics (CPFD), which allows the representation of large multiphase industrial complexes with a number of particles of a magnitude of 10^{16} while still maintaining a low computational cost. The CPFD software employing the MP-PIC approach is called Barracuda and is the one that is going to be use in the context of this study; the equations used are reported in the following section.

CPFD: Governing Equations

Mass and momentum balance equations are solved for gas and particles by using a hybrid Eulerian-Lagrangian approach; they are described below.

The gas phase is solved as a continuum through the Navier-Stokes equations for mass and momentum in the Eulerian framework:

$$\frac{\partial(\alpha_{g}\rho_{g})}{\partial t} + \nabla \cdot (\alpha_{g}\rho_{g}\overrightarrow{u_{g}}) = 0$$

$$\frac{\partial(\alpha_{g}\rho_{g}\overrightarrow{u_{g}})}{\partial t} + \nabla \cdot (\alpha_{g}\rho_{g}\overrightarrow{u_{g}}\overrightarrow{u_{g}}) = -\alpha_{g}\nabla P + \alpha_{g}\rho_{g}\overrightarrow{g} + \nabla\tau_{g} - F$$
(4)

$$\frac{\partial(\alpha_{g}\rho_{g}\overrightarrow{u_{g}})}{\partial t} + \nabla \cdot \left(\alpha_{g}\rho_{g}\overrightarrow{u_{g}}\overrightarrow{u_{g}}\right) = -\alpha_{g}\nabla P + \alpha_{g}\rho_{g}\overrightarrow{g} + \nabla \tau_{g} - F \tag{4}$$

Where $\alpha_g, \rho_g, \overrightarrow{u_g}$ are the volume fraction, density, and velocity of the gas, respectively, while ∇P is the pressure gradient in the system. The gas stress tensor (τ_g) is described by the following equation, while F represents the momentum exchange rate between gas and solid phase.

$$\tau_g = \mu_g \left(\nabla \overrightarrow{u_g} + \nabla^T \overrightarrow{u_g} \right) - \frac{2}{3} \mu_g \nabla \overrightarrow{u_g} I$$
 (5)

Mass and momentum balance equations for the solid phase are instead given by:

$$\frac{\partial(\alpha_{s}\rho_{s})}{\partial t} + \nabla \cdot (\alpha_{s}\rho_{s}\overrightarrow{u_{s}}) = 0$$

$$\frac{\partial(\alpha_{s}\rho_{s}\overrightarrow{u_{s}})}{\partial t} + \nabla \cdot (\alpha_{s}\rho_{s}\overrightarrow{u_{s}}\overrightarrow{u_{s}}) + \nabla \tau_{s} + \alpha_{s}\nabla P$$

$$= \alpha_{s}\rho_{s}\overrightarrow{g} + \iint fm_{p}D(\overrightarrow{u_{g}} - \overrightarrow{u_{p}})dm_{p}du_{p}$$

$$- \nabla \left[\iint fm_{p}(\overrightarrow{u_{p}} - \overrightarrow{u_{s}})(\overrightarrow{u_{p}} - \overrightarrow{u_{s}})dm_{p}du_{p} \right]$$
(6)

in these, the mean solid velocity $(\vec{u_s})$ and solid volume fraction (α_s) are defined by:

$$\overrightarrow{u_s} = \frac{1}{\alpha_s \rho_s} \iint f m_p \overrightarrow{u_p} dm_p du_p \tag{8}$$

$$\alpha_s = \iint f \frac{m_p}{\rho_s} dm_p du_p \tag{9}$$

$$\alpha_g + \alpha_s = 1 \tag{10}$$

In the MP-PIC method, particles with same properties at a given time t are grouped in parcels and their properties are interpolated on the Eulerian grid to solve the solid phase equations. Once the equations are calculated, the Eulerian grid properties, like gas velocities, gas pressure or solid stress gradient are interpolated into the parcels to update their position [29]. In the momentum balance equation, f is the particle probability distribution function which is computed with the Liouville equation for particle position:

$$\frac{\partial f}{\partial t} + \nabla \cdot \left(f \overrightarrow{u_p} \right) + \nabla_{\overrightarrow{u_p}} \cdot \left(\frac{d\overrightarrow{u_p}}{dt} \right) = 0 \tag{11}$$

where $\nabla_{\overrightarrow{u_p}}$ is the divergence operator with respect to velocity. Finally, D is the drag function [27].

4.1.2 Drag Models

As said earlier, it is necessary to correctly model interactions between particles and fluid by using closure equations and, in particular, one that has a great impact is the drag model. The models can be divided between homogeneous and heterogeneous: the first ones are used for homogeneously dispersed solids while the second takes into account the existence of phases with different solid density.

TFMs with a coarse grid have reportedly failed to predict the hydrodynamics of the reactor, especially for Geldart A particles. A fine grid and a small time step has to be used (grid size approximately 2-4 particle diameter for BFB or 10 particle diameters for CFB). Although, fine grid simulations are computationally very expensive. For this reason, various heterogeneous, or sub grid, models have been developed, and they are differentiated in four categories based on the derivation method: fine-grid KTGF based on Two-fluid simulations, fine-grid CFD-DEM simulations, particle-resolved direct numerical simulations (PR-DNS) of cluster configurations or moving particles extracted from the experimental tests and mesoscale-structure-based methods [30].

On the contrary, the impact of the choice between homogeneous or heterogeneous has been found to be lower in CPFD simulations due to the possibility to introduce a PSD for the solid [26]. Also, Karimipour et al. found that the choice of the model has a lesser impact if compared to other parameters, like the grid size [24].

Following the descriptions of the drag models simulated in this study are reported, of which Gidaspow, WenYu-Ergun, Tenneti and Beetstra are homogeneous and EMMS and Radl et al. are heterogeneous. The description are taken from the Barracuda User Manual [31].

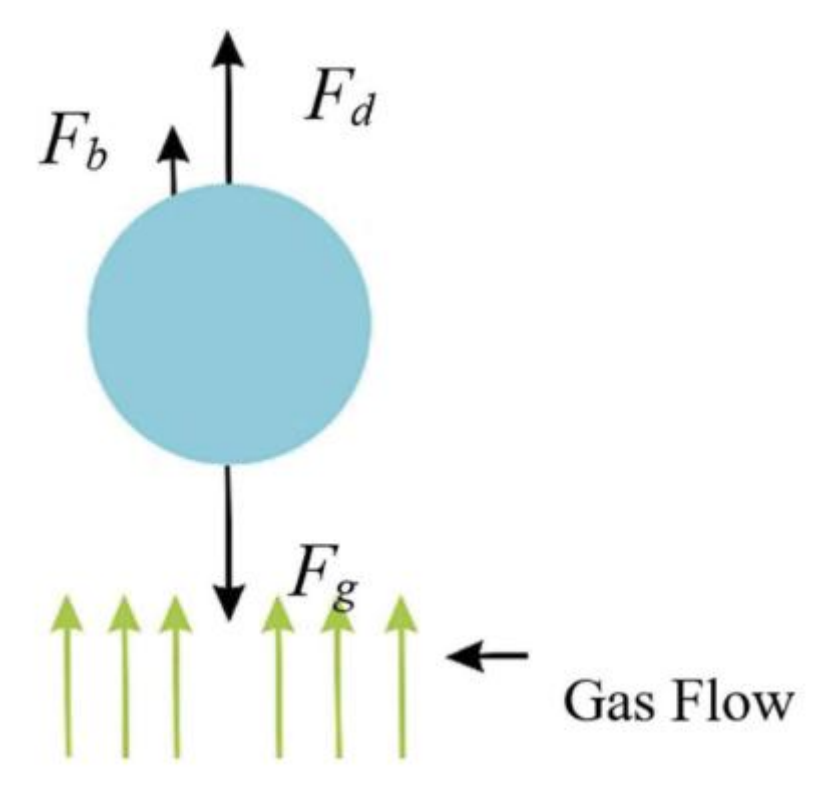


Figure 4.1: Balance of forces on the particle [32]

GIDASPOW

This drag model [33] uses the WenYu correlation in diluted phase and the Ergun correlation at denser ones.

$$F(\phi, Re) = \begin{cases} F_{WY} & \phi \le 0.2 \\ F_s & \phi > 0.2 \end{cases}$$
 (12)

Where F_{WY} is the Wen and Yu drag function F_{ε} is the Ergun drag function with $c_0 = 1.75$ and $c_1 = 150$; they are respectively defined by the following functions:

$$F_{WY} = \begin{cases} F(\phi, Re) = F_{sp} \cdot \theta_f^{-3.65} \\ F_{SP} = \begin{cases} 1 + 0.15Re^{0.687} & Re \le 1000 \\ 0.44\frac{Re}{24} & Re \le 1000 \end{cases} \\ F_e = F(\phi, Re) = \frac{c_0 \cdot Re + c_1 \cdot (1 - \theta_f)}{18 \cdot \theta_f^2} \end{cases}$$
(13)

$$F_e = F(\phi, Re) = \frac{c_0 \cdot Re + c_1 \cdot (1 - \theta_f)}{18 \cdot \theta_f^2} \tag{14}$$

WENYU-ERGUN

This model uses the same approach as the Gidaspow although the blending between dense and diluted phase is different.

$$F(\phi, Re) = \begin{cases} F_{WY} & \phi < c_1 \cdot \theta_{CP} \\ (F_e - F_{WY}) \cdot \left(\frac{\phi - c_1 \cdot \theta_{CP}}{c_0 \cdot \theta_{CP} - c_1 \cdot \theta_{CP}}\right) + F_{WY} & c_1 \cdot \theta_{CP} \leq \phi \leq c_0 \cdot \theta_{CP} \\ F_e & \phi > c_0 \cdot \theta_{CP} \end{cases}$$
(15)

Where F_{WY} and F_e are the Wen and Yu and the Ergun drag function, respectively, defined earlier, θ_{CP} is the particle (or bubble) volume fraction at close pack. $c_0 = 0.85$ is the dense blending limit, $c_1 = 0.75$ is the dilute blending limit, $c_2 = 2$ (as for c_0 in Ergun) and $c_3 = 180$ (as for c_1 in Ergun).

EMMS-YANG-2004

The Energy Minimisation Multi-Scale model EMMS-Yang-2004 is based [34] on and [35]. The EMMS-Yang-2004 model constants were generated for the following conditions based on the Li and Kwauk experiment.

- Air at atmospheric conditions
- 54 micron mono-sized particles
- Particle density of 930 kg/m3
- Fluid Superficial Velocity of 1.52 m/s
- Solids Flux of 14.3 kg/m2/s

$$w = \begin{cases} -0.576 + \frac{0.0214}{4(\theta_f - 0.7463)^2 + 0.0044} & 0.74 \le \theta_f < 0.82 \\ -0.0101 + \frac{0.0038}{4(\theta_f - 0.7789)^2 + 0.0040} & 0.82 < \theta_f \le 0.97 \end{cases}$$
(16)
$$-31.8295 + 32.8295\theta_f & 0.97 < \theta_f \le 1 \end{cases}$$
$$F(\phi, Re) = \begin{cases} \frac{150(1 - \theta_f) + 1.75Re}{18\theta_f^2} & \theta_f < 0.74 \\ (1 + 0.15Re^{0.687})w & \theta_f \ge 0.74 \text{ and } Re < 1000 \\ 0.44\frac{Re}{24}w & \theta_f \ge 0.74 \text{ and } Re \ge 1000 \end{cases}$$
(17)

TENNETI

The Tenneti drag formula [36] includes buoyancy force due to average pressure gradient in the system accounted for as an additional voidage term $(1 - \phi)$.

$$F_{isol} = \begin{cases} 1 + 0.15Re^{0.687} & Re \le 1000\\ 0.44\frac{Re}{24} & Re \le 1000 \end{cases}$$
 (18)

$$F_{\phi} = \frac{5.81\phi}{\left(1 - \phi\right)^3} + 0.48 \frac{\phi^{\frac{1}{3}}}{\left(1 - \phi\right)^4} \tag{19}$$

$$F_{\phi,Re} = \phi^3 Re(0.95 + \frac{0.61\phi^3}{(1-\phi)^2})$$
 (20)

$$F(\phi, Re) = (1 - \phi) \left[\frac{F_{isol}}{(1 - \phi)^3} + F_{\phi} + F_{\phi, Re} \right]$$
(21)

BEETSTRA

The Beetstra drag model is based on the work of Beetstra et al. [37]. The drag model is given by:

$$B_1 = \frac{10\phi}{\theta_f^2} \tag{22}$$

$$B_2 = \theta_f^2 (1 + 1.5\phi^{0.5}) \tag{23}$$

$$B_3 = \frac{0.413Re}{24\theta_f^2} \tag{24}$$

$$B_4 = \theta_f^{-1} + 3\theta_f \phi + 8.4Re^{-0.343} \tag{25}$$

$$B_5 = 1 + 10^{3\phi} Re^{(-0.5 - 2\phi)} \tag{26}$$

$$F(\phi, Re) = B_1 + B_2 + \frac{B_3 B_4}{B_5}$$
 (27)

RADL ET AL. 2014

The Radl-Sundaresan drag model comes from the work of Radl and Sundaresan [38]. It is obtained from the Beetstra model by multiplying a factor, which allows the drag model to consider the coarse-graining effects as a function of grid size, fluid, and particle properties.

$$v_t = \frac{(\rho_p - \rho_f)gd_p^3}{18\mu_f} \tag{28}$$

$$Fr = \frac{v_t^2}{gd_p} \tag{29}$$

$$L_c = \frac{v_t^2 F r^{-\frac{2}{3}}}{g} \tag{30}$$

$$f_s = V^{\frac{1}{3}} \tag{31}$$

$$f\left(\phi, \frac{f_s}{L_c}\right) = 1 - \frac{h(\phi)}{\frac{a(\phi)L_c}{f_s} + 1} \tag{32}$$

$$F\left(\phi, Re, \frac{f_s}{L_c}\right) = f\left(\phi, \frac{f_s}{L_c}\right) F_{BVK}(\phi, Re) \tag{33}$$

Where $a(\phi)$ and $h(\phi)$ are two algebraic expressions defined in the paper and the rest of the terms that appear are the following:

- v_t is the terminal velocity in creeping flow
- g is the gravitational force magnitude
- d_p is the particle diameter

- μ_f is the fluid viscosity
- Fr is the Froude number
- L_c is the characteristic length
- *V* is the volume of the grid/cell
- f_s is the filter size
- $\frac{f_s}{L_c}$ is the dimensionless filter size
- f is the multiplication factor
- F_{BVK} is the drag force obtained from the Beetstra model

4.1.3 Other Simulation Parameters

These simulation parameters are usually adjusted to be able to fit the available data.

GRID REFINEMENT

A good grid should be accurate in representing all the main interest points of the structure, it should have a sufficient enough resolution to represent correctly the particle-fluid interaction, and it should be as uniform as possible for a stable simulation, therefore gradual changes should be made from zones of high resolution to zones of lower one. Finally, it is desirable to keep the number of cells as small as possible while still accounting for all the precedent characteristics, to obtain the results in a smaller amount of time.

In the Barracuda software the grid is created starting from the generation of a uniform grid on a parallelepipedal area around the designed geometry. It is then possible to adjust the lines to obtain a greater refinement in specific areas of interest and important details and, in the end, only the cells within the designed domain are taken into account for the calculation, which leads to a differentiation between total cells and real cells.

TIME STEPS

The Courant-Friedrichs-Lewy (CFL) number is a dimensionless measure of how far fluid travels in a single time step. A 3-dimensional number is computed, for each direction:

$$CFL = \frac{u \cdot \Delta t}{\Delta x_{cell}} \tag{34}$$

Where Δx_{cell} is the cell dimension in the current direction, u is the velocity of the fluid and Δt is the time step. In order to maintain the stability, accuracy, and speed of the calculation the time step is automatically adjusted to keep the CFL within the defined values, which are set as a minimum of 0.8 and a maximum of 1.5 as a default.

RESTITUTION COEFFICIENT

The restitution coefficient (RC) depends on the particle's physical properties such as size, shape, roughness, among others, and it is then difficult to measure it experimentally, but it is usually adapted based on the simulation results and the available data. It accounts for the dissipated kinetic energy related to collisions and it ranges from a value of 0 for perfectly inelastic collision to unity for elastic collision with no dissipation of kinetic energy.

An increase of this coefficient leads to lower bed expansions and a lower relative height of fluctuations since a greater value leads to the formation of smaller bubbles [39].

This parameter is present on Ansys Fluent but not used on the CPFD software Barracuda.

SOLID PHASE STRESS TENSOR

In the CPFD method, instead of the restitution coefficient, contacts and collisions between particles are modelled through a particle stress function:

$$\tau(\theta_p) = \frac{10 \cdot P_s \cdot \theta_p^{\beta}}{max[\theta_{cp} - \theta_p, \varepsilon \cdot (1 - \theta_p)]}$$
(35)

where P_s is a constant with units of pressure (1 Pa), θ_{cp} is the solid volume fraction at close pack, β is a constant between 2 and 5 and a value of 3 was utilized in this study, and ε is a very small number (10⁻⁸).

The model should have negligible influence on the particles when they are in the dilute phase, while it should affect the particles in or travelling towards a close pack region by preventing them entering it and redirecting them.

SPECULARITY COEFFICIENT

It is important to well define the interactions between particles and walls and, for that, the Johnson and Jackson solid phase wall boundary condition is used. The tangential velocity of the solid phase is expressed as follows:

$$u_{p,w} = -B \frac{\partial u_{p,w}}{\partial n} \tag{36}$$

$$u_{p,w} = -B \frac{\partial u_{p,w}}{\partial n}$$

$$B = \frac{6 \cdot \alpha_{p,max} \cdot \mu_{p}}{\sqrt{3} \cdot \sqrt{\theta} \cdot \pi \cdot SC \cdot \rho_{p} \cdot \alpha_{p} \cdot g_{0}}$$
(36)

where α_p , ρ_p , θ and μ_p are the volume fraction, density of solid phase, granular temperature and viscosity of solid phase p, respectively, and g₀ is the radial distribution function. B is the slip coefficient, and it is inversely proportional to the specularity coefficient (SC) which is an empirical parameter qualifying the nature of particle-wall interactions and which ranges from 0 (perfect specular collisions) to 1 (perfectly diffuse collision). A SC of 1 is often employed as a no-slip boundary condition, although Zhong et al. [40] reported a nonnegligible difference related to the fact that the tangential velocity in the Johnson and Jackson solid phase is hardly to be zero, unlike the no-slip condition, and therefore a weaker interaction between particles and wall is found.

This parameter is present in the CFD models.

MOMENTUM RETENTION PARAMETERS (MRP)

The interactions between walls and particles in the CPFD are instead described through the normal-to-wall and tangent-to-wall momentum retention parameters. The first one is the fraction of momentum retained by the particle after an impact normal to the wall, while the second one is the retention after an impact on a direction tangential to it. The velocity of the particle after the impact is described by the following formula:

$$|u^{n+1}| = [(r_T - r_N) \cdot (1 - \cos \theta) + r_N] \cdot |u^n|$$
(38)

Where $|u^{n+1}|$ and $|u^n|$ are the velocity of the particle at the instant n and n+1, before and after the impact respectively. r_T and r_N are the normal and tangential parameters and θ is the impact angle [29]. Usually, the normal parameter is lower than the tangential one especially for softer particles, while it can be set equal to it in the case of harder ones.

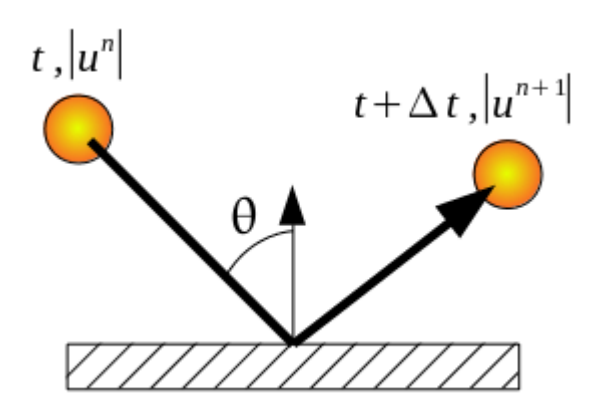


Figure 4.2: Model for momentum retention

DIFFUSE BOUNCE

The diffuse bounce completes the momentum retention parameters in the particle-wall interaction for the CPFD by applying a scatter function to the particles impacting the wall. The value ranges from 0 to 5, with the lowest indicating no scatter and therefore all the particles impacting the wall with the same velocity vector are going to leave the wall in the same direction (the parameter only impacts the direction but not the overall magnitude). The default value is 0, but a bigger one is often used to take into account the not perfect sphericity of the particles and the not perfect smoothness of the walls. The following table shows the angle variation in function of the parameter.

	Maximum	
Diffuse Bounce	$ heta_{scatter}$ (+/-)	
0	0.0°	
1	4.0°	
2	8.0°	
3	12.0°	
4	15.8°	
5	19.5°	

Figure 4.3: Angle variation in function of the Diffuse Bounce

5 Objectives

5.1 Bibliographic Review

The first objective is a state-of-the-art report with the double intent of:

- Establishing the advancement status of research on the topic of simulation of fluidized beds with a pulsing gas inlet as well as determining the trend of interest generated by it in time and whom are the main actors behind it.
- Retrieving important information related to the main numerical models used for representation of Geldart A particles fluidized beds, the closure equations chosen and the main simulation parameters.

5.2 Simulation Approach

The second objective of this internship is to set up a computational model able to reproduce the main experimental data obtained at IFPEN, in their pilot scale reactor, via the use of the CPFD software Barracuda. The goal is to obtain a well-established model for the representation of the fluidization phenomena inside the IFPEN reactor and to reproduce the impact of different frequencies of pulsation being applied to the inlet air flowrate.

A fine tuning of the simulation parameters and model hypothesis for a previously developed model of the vessel is going to be performed. The model presents the geometry and the details of the structure, the grid and boundary conditions files for a continuous case but it does not account for the mass transfer, so no Helium is present in the configuration, nor the possibility to add a pulsation to the inlet. More specifically, the fine tuning will focus on the impact of the drag model, the solid volume fraction at the solid inlet, and the momentum retention parameters.

Once the model is perfected for the continuous case, the possibility to add a pulsative inlet is implemented and frequencies at 1, 3, 5 and 7 Hz are applied to verify their fitting of the experiments.

The results of both Objective 1 are shown in section 6 while the ones of Objective 2 are in sections 7 and 8.

6 Systematic Literature Review

6.1 Methodology

The systematic review was organized in three steps and led on the multidisciplinary database Scopus. The chosen string line took into account the differences in pronunciation and the specificity of the researched topic searching for "("fluidiz*" OR "fluidis*") AND ("cfd" OR "simul*" OR "numeri*" OR "comput*" OR "modelling" OR "modelling") AND ("puls*" OR "oscillat*")" on the title, abstract and keywords and adding another constraint by imposing the presence of "("FCC" OR "Geldart A" OR "catal*" OR "Geldart-A")" in all fields of the document. The search was limited to English language documents, it led to a total of 126 articles, and it is current as of April 15, 2025.

The first step consisted in retrieving the document from the Scopus website, including the title, publication year, author and Country. In the second step a selection of the papers related to the chosen topic was conducted, keeping those papers that were focusing on gas-solid fluidized beds and disregarding the ones including other phases, focused on the modelling of reaction kinetics, reviews or books. In the last step, the papers where subdivided based on the type of solids used, according to the Geldart classification and concentrating mostly on the ones with type A particles. For these papers, information related to the main simulation parameters used was retrieved, together with the software, the closure relation for the drag force, the CFD model, and whether they were using a pulsating or a continuous gas inlet. Finally, other articles relevant for the research process were added through the reviews found or the citations. Figure 6.1: Sankey Diagram of the Research Results shows the results of the separation after each phase.

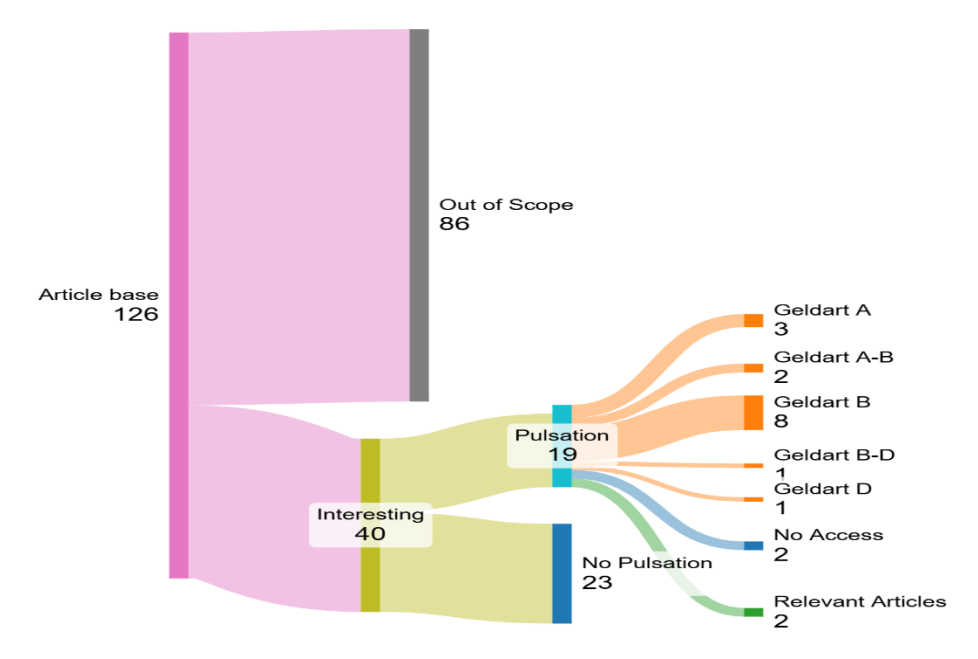
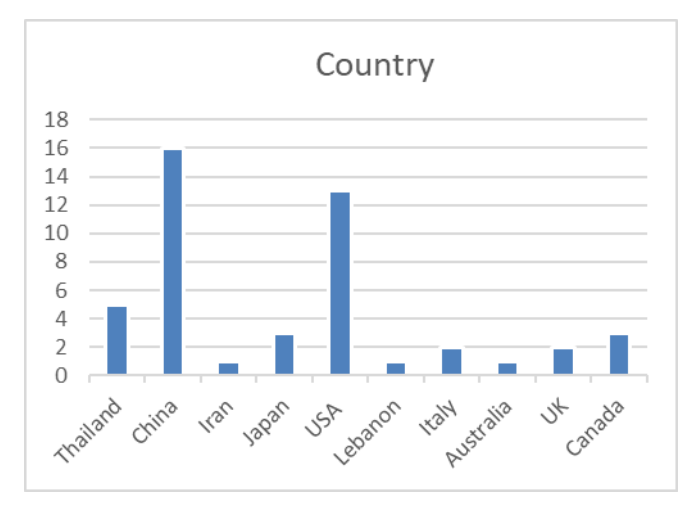


Figure 6.1: Sankey Diagram of the Research Results

6.2 Results of Systematic Review

Out of the 126 documents, retrieved on the first step, only 40 satisfied the eligibility criteria during the second step, and the great majority of them was almost equally subdivided between the use of Geldart A and Geldart B solids. Looking at the number of publications per year, in Figure 6.3, it is possible to see an overall increasing interest with 26 papers being published in the last 10 years with two peaks in 2017 and 2021, although this interest appears, for the moment, in descent; China, USA and Thailand respectively were the greatest contributors to the field with 34 papers having at least one of the authors coming from a university or institution from those Countries, as shown in Figure 6.2. Less than half of the papers (15) were using a bed Geldart A type of particles, and only 3 were applying a pulsating inlet for the fluidization.

From these 15 papers, various information regarding the model, the software and the main parameters was obtained. Almost the totality of the authors used a TFM closed by the KTGF and only two used a DPM or a Dense Discrete Particle Model (DDPM); the preferred software was Ansys Fluent (used in 13 papers) while the M-FIX was the second one (2 papers) and there were some experiences with the CFX4.1 and a modified Los Alamos K-FIX software. The most used drag models are reported in Figure 6.4, where "others" refers to the models that were not described. About the simulation parameters, a value of the specularity coefficient lower than 0.1 (free slip condition at the wall) was preferred in five of the papers, only in three it was higher (in one case in the context of a parametric study) and it was not specified for seven papers; the data is reported in Figure 6.5. The particle-particle restitution coefficient value was usually chosen at 0.9 or 0.95 in about half of the articles and 0.7 or 0.8 in the other half (only in one case it arrived to 0.6), while the particle-wall RC never went down 0.9; in six documents the two parameters were set at equal values and in seven papers the value was not reported at all. The timestep has been reported to be an important factor, especially for CFD simulations [41], and it was then reported in these results. The value ranges from 10⁻⁵ to 10⁻³ with five papers using a value at 10⁻⁴, three at 10⁻⁵ and two at 10⁻³; in a third of the results, the value was not specified.



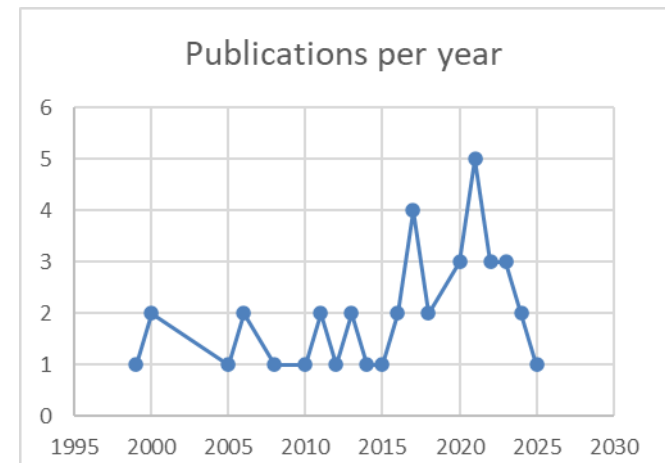


Figure 6.2

Figure 6.3

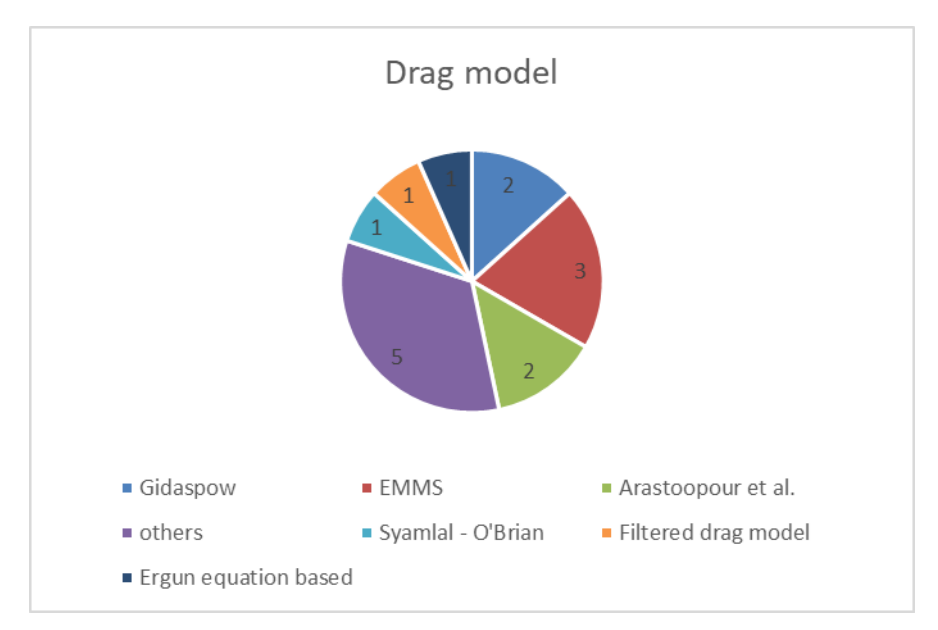


Figure 6.4

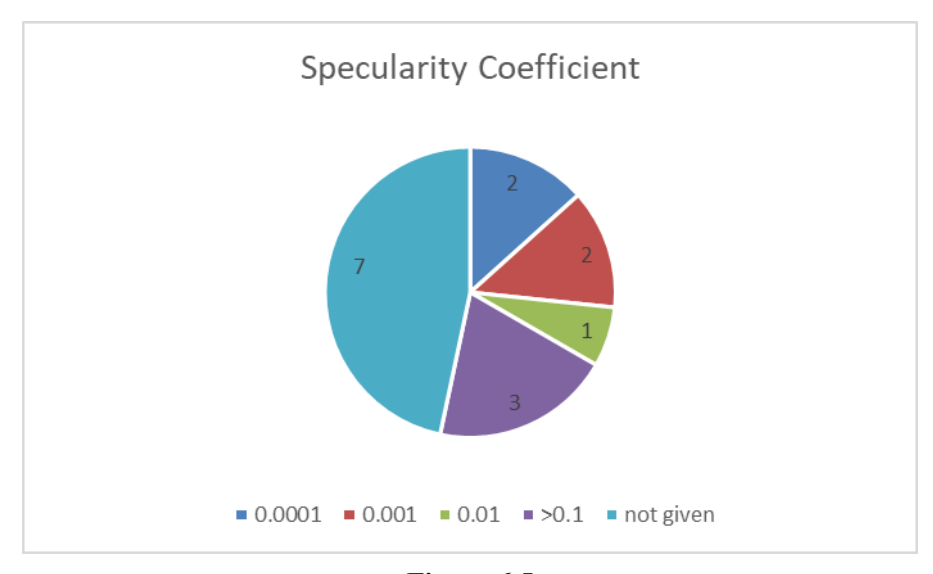


Figure 6.5

6.2.1 Description of Selected Papers with Pulsation

In this section the main findings of the three papers that investigated a pulsing inlet are going to be explored with a focus on key aspects like the CFD and the drag models used, the simulation parameters, and the interpretation of the results from the authors.

Shah et al. [42] investigated the impact of amplitude and frequency of a rectangular pattern pulsating flow on two gas-solid flow conditions: a cold flow with FFC catalyst and air on the reactor proposed by Knowlton et al. as PRSI challenge problem, and a reactive flow with FCC catalyst and vacuum gas oil (VGO) vapour, experimentally investigated by Derouin et al. [43]. Both flows were simulated using a 2D geometry (with different dimensions) and described via the TFM using the KTGF for the closure equations, on the Ansys Fluent software. The drag force was described with the EMMS model and the SC, the RC, and time step are reported to be defined respectively as 0.0001, 0.7 and 0.0005 s. Five cases for each flow were simulated, one with a continuous inlet (used to validate the simulation setup) and the others at different pulsation frequencies (2, 1, 0.5 or 0.25 Hz) and it was found that the

pulsation allows for a greater homogeneity in the radial profiles (of the catalyst volume fraction, temperature and VGO and gasoline mass fractions) than the continuous flow. Also, at higher frequencies, the impact of the pulse amplitude is minor, while at low frequencies a higher amplitude leads to a greater accumulation of solids on the walls, leaving the core region unaffected. Finally, the pulsating flow leads to a higher conversion and yield in the first few meters of height.

Chaiwang et al. [44] reproduced the same reactive flow as Shah et al., looking at their results for the validation of their 3D model. They also investigated amplitude and frequency as well as the waveform type, using a KTGF-TFM approach with the EMMS drag model. The SC was equal to 0.0001, the RC to 0.7 and the time step was set to 0.001. The simulation results showed that the parameters with the most significant impact on the response parameters were the frequency and waveform type. A higher frequency increased the turbulent behaviour in the system, while changing from a square-shaped waveform to a sine-shaped one led to increased conversion and yield levels since the changing at minimum and maximum values results in a more continuous transition operation.

Finally, Xiaoxue et al. [45] studied the impact of a pulsating inlet flow, at different frequencies and amplitudes, on the cluster distribution frequencies and existence times in the riser of a circulating fluidized bed reactor with the following dimensions: 10 meters in height and 76 mm in diameter. The adopted CFD model was once again the KTGF-TFM but with two different drag laws used for the dense and the diluted sections of the reactor; in the diluted part, the Huilin-Gidaspow correlation was used while, in the dense section, the Dynamic Cluster Structure-Dependent (DCSD) model was preferred. The SC is fixed at 0.5, the RC at 0.95 and an adaptative time step was chosen, varying on a range from 10⁻⁵ and 10⁻³ seconds. The authors found that the cluster diameter, solid volume fraction, existence time fraction, and the number fraction were all higher for a continuous gas inlet, while they were the smallest for a pulsating flow of amplitude 1 m/s and a frequence of 4 Hz. They were then able to conclude that amplitude and frequency of pulsation play an important role on the regulation and control of agglomerate formation in fluidized beds, as we can see in Figure 6.6 and Figure 6.7.

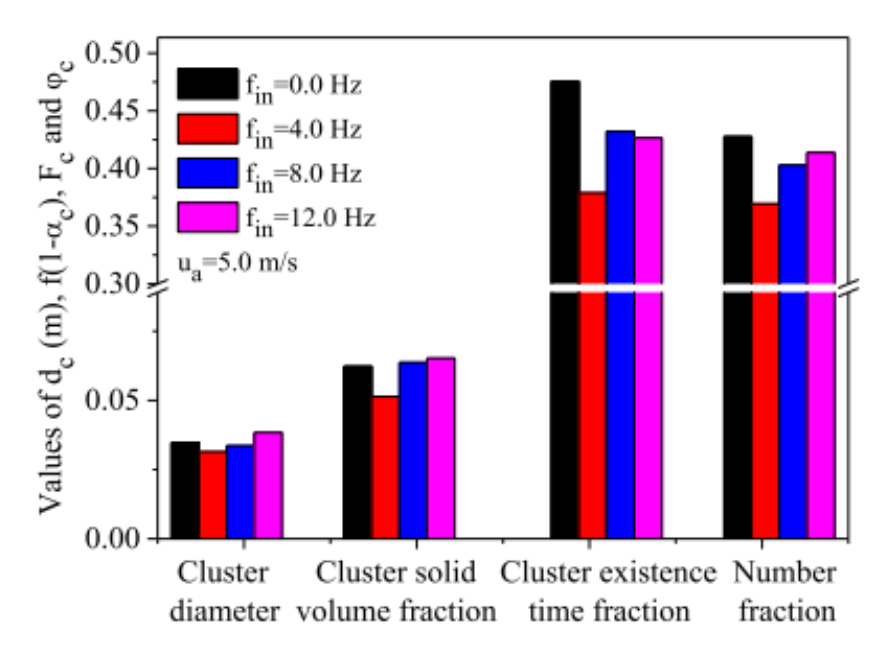


Figure 6.6: Cluster diameter, solid volume fraction, existence time fraction, and number fraction in function of different pulsation frequencies. [45]

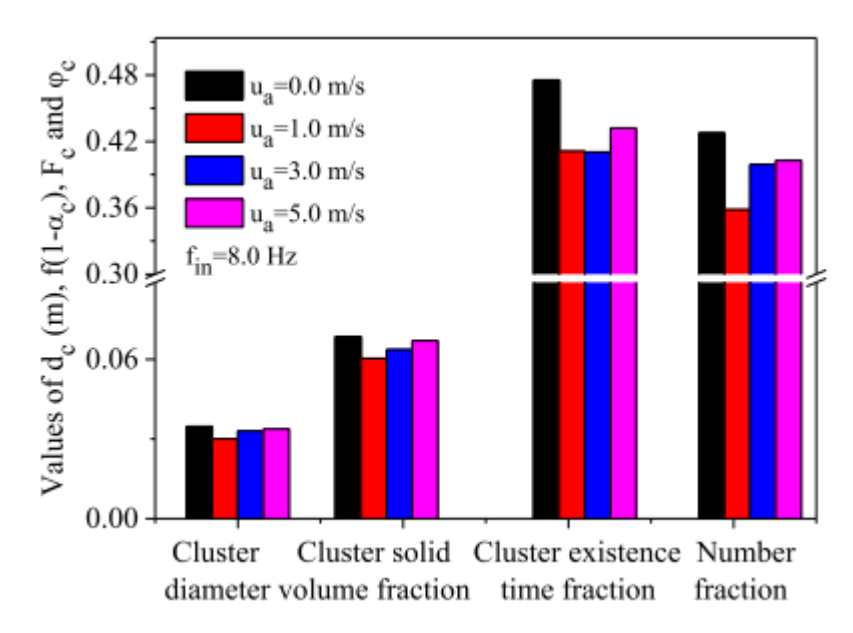


Figure 6.7: Cluster diameter, solid volume fraction, existence time fraction, and number fraction in function of the amplitude of pulsation at a fixed frequency of 8 Hz. [45]

6.2.2 Other Relevant Articles

The following articles have been found through other works retrieved from the literature review or from personal research and have been included on the basis of their relevance to the study, even if not directly treating the pulsation method.

Gao et al. in 2017 [30] studied the impact of the drag model choice on the representation of fluidized beds with coarser grids. Four different fluidization regimes were chosen, each on a specific reactor: bubbling regime on the "travelling fluidized bed" (Dubrawski et al. [46]) with a superficial gas velocity of 0.4 m/s, turbulent regime (Venderbosch 1998) with a velocity of 0.8 m/s, fast fluidization regime (Wei et al. [47]) at 3.25 m/s, and dilute phase transport (Andreux et al. [48]) at 7.0 m/s. The first reactor takes his name from an experimental apparatus composed of a single modular fluidized bed unit, instrumentation and components, together with FCC and Silica Sand particles, which travelled to different universities for experimentation [46], and therefore there are various measures obtained with different techniques. About the representation of the drag forces, eight models have been chosen: Gidaspow ([49]), BVK (Beetstra et al., [37]), TGS (Tenneti et al., [36]), Igci (Igci et al., [50]), Radl (Radl et al., [38]), Sarkar (Gao et al. [30]), MMS (Mehrabadi et al., [51]), EMMS (Li and Kwauk, [35]). A distinction has been made between homogeneous drag models (the first three), which work well for homogeneously dispersed solid, and sub-grid or heterogeneous models (the last five) which offer a better representation of the bed in the case of the presence of meso-scale structures, such as clusters of particles or bubbles especially for certain types of solids and fluidization regimes.

The regime of interest for this review is the bubbling one, so the results reported are related to it. The authors found that, except for the MMS drag model, the heterogeneous drag models were representing well the experimental data, as shown in Figure 6.8, while the homogeneous ones were overpredicting the bed void fraction. Also, on the radial void fraction, the Sarkar, Igci and Radl models were closer to experimental data than the EMMS. About the bubble behaviour, again only the Sarkar, Igci and Radl correctly predicted it while other models predicted a fluidization behaviour similar to a turbulent fluidized bed. Finally, concerning the

bed height, the errors of heterogeneous drag models were less than 10%, and the results are reported in Figure 6.9.

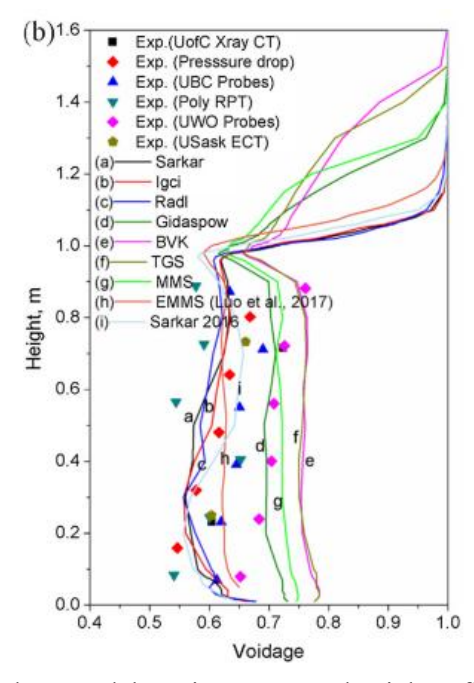


Figure 6.8: Impact of drag model on time-averaged axial profiles of bed void fraction

Drag models	Predicted expansion height, m	Exp.	Errors (%)
Sarkar	1.084	1.100	-1.45
Igci	1.086		-1.27
Radl	1.089		-1.00
Gidaspow	1.288		17.09
BVK	1.455		32.27
TGS	1.415		28.63
MMS	1.209		9.91
EMMS (Luo et al., 2017)	1.152		4.73
Sarkar 2016	1.104		0.36

Figure 6.9: Predicted expansion heights for the bubbling fluidized bed in function of the drag model

Vashisth et al. in 2014 [26], reproduced the same bed of Gao et al. [30] ("travelling fluidized bed", [46]) and studied the impact of the choice of model in the results; the bed was represented using CFD with the TFM and CPFD. The authors tested five different drag models for the CFD simulation: Wen Yu (Yu et al., [52]), Wen Yu/Ergun equation (Gidaspow, [49]), two versions of the EMMS (Shi et al., [53] and Hong et al., [54]), and the newly developed Force Balance (FB) model (Motlagh et al., [55]) which is introducing the effect of the particle agglomeration on the drag force and considering non perfectly spherical particles. It was found that the drag model plays an important role on the estimation of the bed height and particle concentration in the dense phase and that it needs to be corrected through a parameter tuning to be applied to a bed of Geldart A particles. The FB model showed results in good agreement with the experimental ones thanks to the consideration of the interparticle van der Waals forces, expected to delay bubbling and to extend the range of homogeneous fluidization. The results of the FB model were close to the ones coming from CPFD, even though the last one does not take into account the cohesive forces, and a possible explanation could be coming from the PSD. For the CPFD, the PSD is in fact specified (contrary to the CFD simulations) and it was shown that the dimension of the agglomerates considered in the

FB model was not surpassing the biggest diameter of the PSD, meaning that the effects on the gas-particle forces were similar. CPFD was therefore able to predict reasonable bed heights without altering existing drag models.

6.3 Conclusions

Attentive research on the Scopus website led to retrieving a total of 126 articles of which about two thirds were out of scope, while the vast majority of the rest were treating solids other than the Geldart A particles studied in this document, drawing the attention to three papers.

Some interesting information could be retrieved regarding the closure equations of the models used, although all papers were modelling with a CFD-TFM, and regarding the main simulation parameters like the SC, the RC and the timestep. It was found that a free slip condition at the wall is preferred (meaning a very low SC), that the RC is for the greater part set above 0.9 and that the timestep has an important influence on the CFD simulations and has to be chosen at low value (usually between 10^{-5} and 10^{-3}).

The main results from the three Geldart A papers showed that pulsation increases the homogeneity of the bed, the conversion of the reactants and the control of agglomeration. Frequency, amplitude and shape of the pulsation were found to be the most influential parameters. In particular, some papers presented high frequencies to increase the turbulence in the bed, and therefore beneficial, while others found greater cluster control at lower ones.

Finally, the last papers showed the importance of the choice of the drag model and offered a comparison between the two different models, CFD and CPFD.

In conclusion, the studies present in literature regarding pulsating fluidized beds of Geldart A particles are still scarce and have been neglected in favour of beds that are less problematic in terms of agglomeration and fluid dynamics. The results found show some discrepancies, but they are, for the most, in agreement regarding the parameters choice and the necessity to adapt the closure equations to the specific case (particle type and fluidization regime). Eulerian-Eulerian approaches have been preferred in the vast majority of the papers and very few of them have employed an MP-PIC approach. With these results, the choice of treating pulsation in beds of Geldart A particles with the CPFD software, undertaken in this internship, is justified and presented in the following sections.

7 Sensitivity Analysis on Continuous Case

This section is dedicated to the fine tuning of the stripper's model under a continuous gas flowrate case.

Information of hydrodynamics in the fluidized bed, such as bed density and bed height, as well as stripping efficiency of Helium were available for solid flux (G_s) equal to 15 kg/m²/s, therefore all the reported results are obtained for this condition.

7.1 Methodology

The first simulations were performed on the pre-existing Barracuda project with the adding of a Helium flowrate at the top inlet, together with the solid one. A trouble shooting of the errors led to a change in the boundary conditions choice and the solid flux.

Once the errors have been accounted for, the following operations were performed:

- The testing of different drag models, each described in section 4.1.2.
- The analysis of the influence of the solid volume fraction at the particle inlet.
- The study of the impact of different values of the momentum retention parameters.

7.2 Simulation Setup

7.2.1 Starting Setup

The geometry has been realized following the real dimensions of the reactor. In the following, Table 7 reports the dimensions and Figure 7.1 and Figure 7.2 show the sketch of the geometry and the detail of the sparger respectively. The mesh has been created starting from a uniform grid of 400,000 cells and setting the refinement lines specifically in the zone of the sparger, which required greater precision.

The fluids (Helium and air) were taken from the predefined ones already present on the Barracuda software, while the solid was defined following the properties of Table 1.

Table 7: Pilot scale reactor dimensions.

Stripper's Geometric Characteristics

Vessel D (m)	0.08
Vessel H (m)	1.2
Dipleg length (m)	0.684
Dipleg D (m)	0.04
Top outlet D (m)	0.04
Bottom outlet D (m)	0.04
Outlets length (m)	0.15
Central tube sparger D (m)	0.0137
Lateral tubes sparger D	0.008
(m)	
Sparger holes D (m)	0.0015
Sparger holes number	10.5

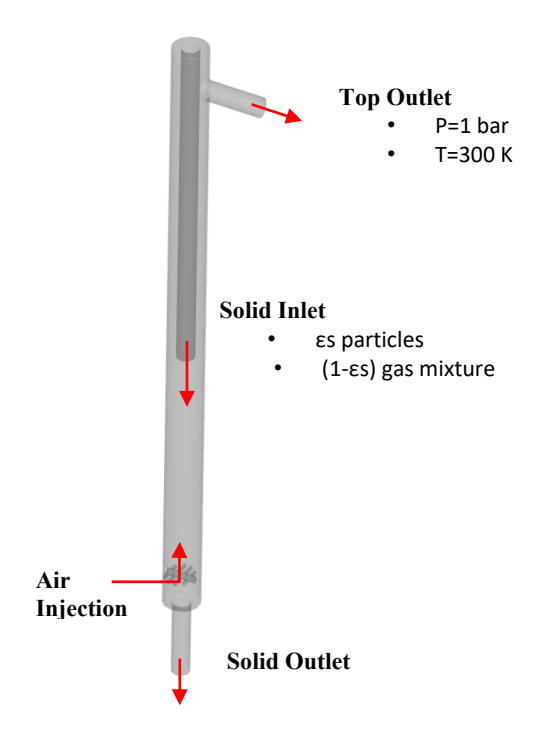


Figure 7.1: Geometry and Boundary Conditions of the simulated bed.

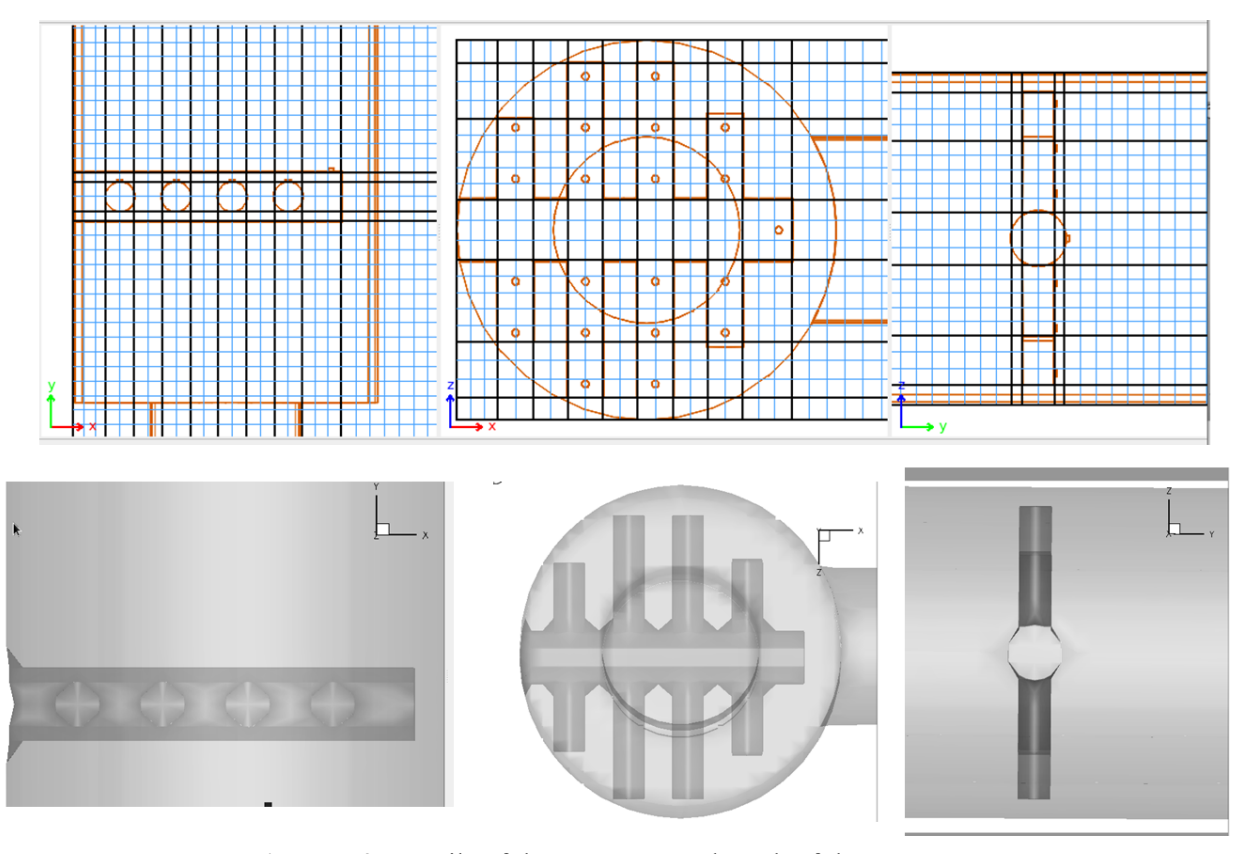


Figure 7.2: Details of the geometry and mesh of the sparger

For this multiphase model, the following boundary conditions have been assigned. For the air injection, 21 injection points have been simulated with a position on the grid as shown in the top central image in Figure 7.2, by the little circles. The velocity of the gas is

assigned at 13.477 m/s, calculated to have a superficial gas velocity of 0.1 m/s in the vessel, with a volume fraction equal to 1.

For the particle inlet, a boundary condition connection has been put in place to be able to recirculate the totality of the solid and of the air coming out of the bottom exit.

For the bottom outlet, an outflow with size filtering has been chosen for the solid, but without a limitation on the size of the particles and with a control on the exit to be able to obtain a solid flow of 0.12874 Kg/s, and a solid volume fraction equal to 0.6. A velocity of 0 m/s was imposed instead for the gas.

For the top outlet a pressure-outlet boundary condition is used with a pressure equal to 1 bar and again an outflow with filtering but no size limitation.

For the walls, a specularity coefficient of 0.2 was used with a diffuse bounce equal to 5 for the particles, and a no slip condition is imposed as a default for the gas phase.

Regarding the initial conditions, volume fraction and bed height have been imposed by looking at the experimental results. So, a bed height of 0.735m with a solid volume fraction of 0.479 have been used.

Finally, the simulation time was chosen at 150 seconds with a time step of 0.001s.

7.2.2 Modifications

The first modification to the starting setup was the adding of a flowrate of Helium at the solid inlet. Looking at the experimental data, the Helium flowrate coming in the stripper was of 0.05 Nm³/h and it has been converted to a mass flowrate, keeping in consideration a temperature of 300K and a pressure of 1 bar, with the following equations:

$$\dot{Q}_{He} = \dot{Q}_{He}^{N} \cdot \frac{p_0 \cdot T}{p \cdot T^{N}} = 1.5456 \cdot 10^{-5} m^3 / s \tag{39}$$

$$\dot{m_{He}} = \dot{Q_{He}} \cdot \rho_{He} = 2.7512 \cdot 10^{-6} Kg/s$$
 (40)

Where p_0 and T_0 are the pressure and temperature in normal conditions (1 atm and 0°C) and ρ_{He} is the density of Helium.

Considering that, from the cyclone dipleg, the solid entering in the unit has a solid volume fraction around 0.4 and that both the flowrates of Helium and of the particles have been fixed, the remaining air flowrate at the particle inlet has been calculated as follows:

$$\dot{m}_{s} = 0.12874 \frac{Kg}{s} \tag{41}$$

$$\dot{Q}_{s} = \frac{\dot{m}_{s}}{\rho_{s} \cdot \varepsilon_{s}} = 1.5645E - 4\frac{m^{3}}{s} \tag{42}$$

$$\begin{cases} \dot{Q}_{g} = \frac{\dot{Q}_{s}}{0.4} \cdot 0.6 \\ \dot{Q}_{g} = \frac{\dot{m}_{air}}{\rho_{air}} + \frac{\dot{m}_{He}}{\rho_{He}} \end{cases}$$

$$(43)$$

$$\begin{cases} m_{air}^{i} = 1.4614E - 4 Kg/s \\ m_{tot}^{i} = m_{air}^{i} + m_{He}^{i} = 1.4889E - 4 Kg/s \end{cases}$$
(44)

Where \dot{Q}_s and \dot{Q}_g are the solid and gas (mixture of air and Helium) volumetric flowrates and from which we obtain a percentage in weight of the gases in the mix equal to 0.98152 for the air and 0.01848 for the He.

The application of this change meant that the particle inlet BC originally used (recirculation of the outlet) was changed to a defined inlet flow composed by 0.4 solid and 0.6 gas mixture with the composition reported earlier.

Finally, the particle flow was changed to better fit the experimental one, and therefore the particle inlet conditions have changed and are reported in the following section. The one used in the experiment is equal to $60 \text{ Kg/m}^2/\text{s}$, referred to the cross-sectional area of the cyclone dipleg.

7.2.3 Final Simulation Setup

The final setup uses the same geometry reported in section 7.2.1, while the boundary conditions are reported in Table 8.

Table 8: Boundary Conditions for Sensitivity Analysis

Boundary Conditions

A • T • 4•	I · · · · · · · · · · · · · · · · · · ·
Air Injection	Injection BC
	• 21 injection points distributed as in Figure 7.2
	• Air velocity equal to 13.477 m/s
	• Air mass flow equal to 2.917E-5 Kg/s
Particle Inlet	Flow BC
	• Composition: 0.4 particles + 0.6 gas mixture (Helium + air)
	Solid
	• $\dot{m}_s = 0.075398 Kg/s$
	Fluid
	• $m_{tot} = 2.2597E - 4 Kg/s$
	• $\%_{\text{wt}}$ air = 0.98783 and $\%_{\text{wt}}$ He = 0.01217
Particle Outlet	Flow BC
	Solid
	• Outflow with size volume filtering (no size limitation)
	• Target solid flowrate = -0.075398 Kg/s
	• Target particle volume fraction (ε) = 0.6
	Fluid
	• Exit velocity = 0 m/s
	• Air mass fraction = 1 (not influent on exit composition)
Top Outlet	Pressure BC
	Solid
	• Outflow with size volume filtering (no size limitation)
	Fluid
	• Pressure = 1 bar
	• Temperature = 300 K
	• Air mass fraction = 1 (not influent on exit composition)

7.3 Results

In this section the main results of this first series of simulations are reported. Firstly, the most appropriate drag model was chosen, secondly the impacts of the solid volume fraction in the

solid flowrate at the inlet were studied and then the momentum retention parameters have been evaluated to obtain results as close as possible to the experiments.

The results are based on the comparison of the bed bulk density and height of the column, calculated starting from equation (2), obtained for the simulated cases with the ones obtained from the experimental data.

All simulations start from the final simulation setup described in section 7.2.3.

7.3.1 Drag Model

The impact of the drag model choice has been tested on five different drag models, of which three are homogeneous models (Gidaspow, Tenneti, Beetstra) and two are heterogeneous (EMMS and Radl-Sundaresan). The results are here reported:

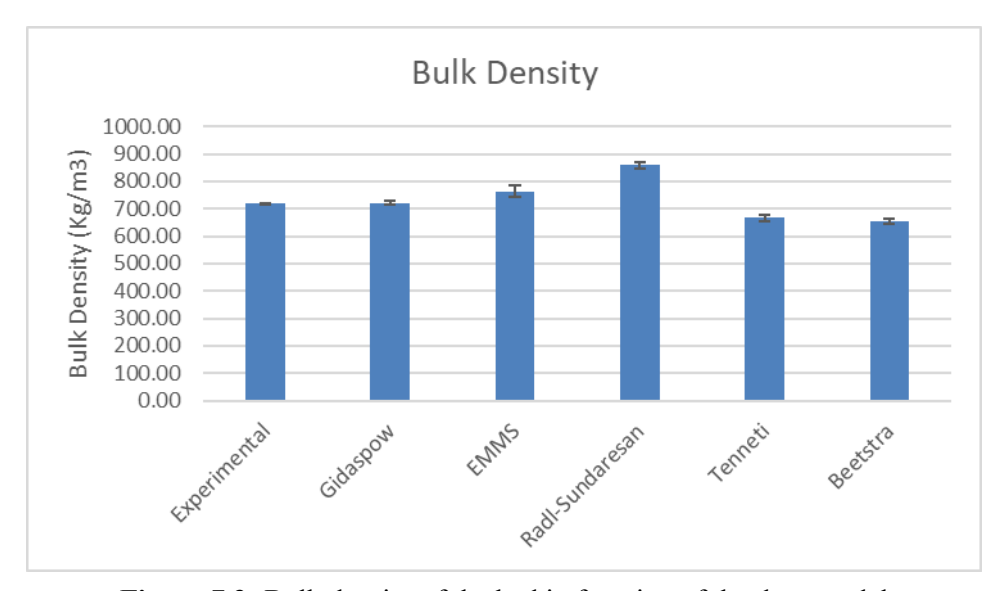


Figure 7.3: Bulk density of the bed in function of the drag model

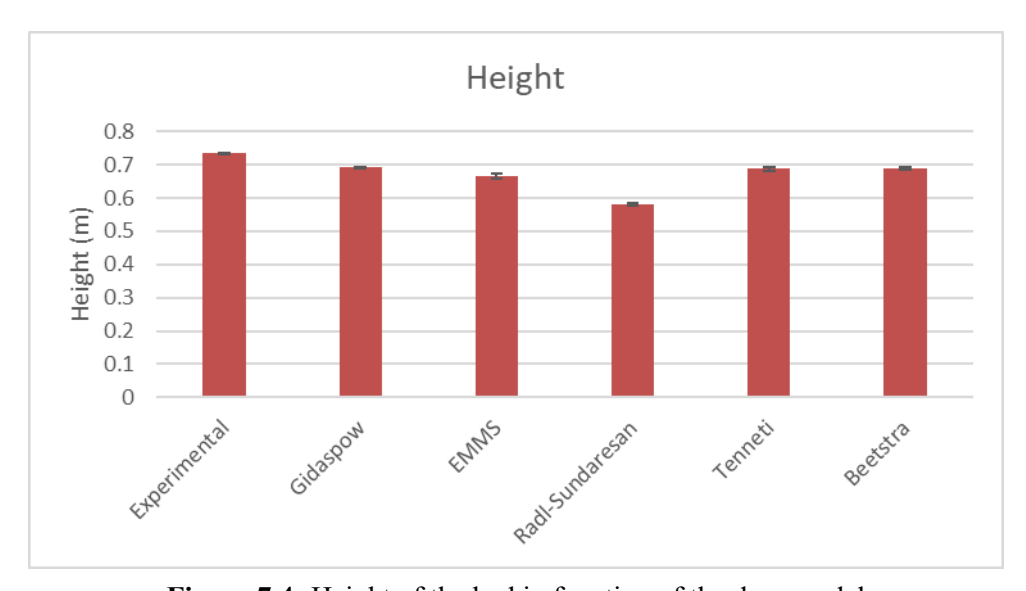


Figure 7.4: Height of the bed in function of the drag model

Looking at Figure 7.3 and Figure 7.4, it is possible to see a moderate impact on the density and height of the bed, with only the Radl et al. model reporting results quite far away from the

experimental ones. These results are in accordance with literature; Córcoles et al. [56] reported in fact a little influence of the drag law on CPFD simulations. Also, Vashisth et al. [26], in comparing results from TFM with heterogeneous drag models and Barracuda, found that Barracuda was obtaining results close to the TFM even without a modified drag law and hypothesized that this was due to the PSD implemented in the CPFD software, as explained in section 6.2.2.

The Gidaspow drag model was therefore chosen for the optimized case due to its proximity to the data and its greater simplicity.

7.3.2 Solid Volume Fraction

Looking at the qualitative results of the bed simulated with an inlet solid volume fraction of 0.4, in Figure 7.5: **Bed hydrodynamics for** \varepsilon **s** = **0.4**it is noticeable a bed overexpansion with a good amount of solid going out from the top outlet of the bed. This behaviour does not match the experimental results, which usually show a bed height of about 0.700 meters, and it is not visible from the equation for the calculation of bed height. This is due to the fact that the density is assumed constant throughout the bed and equal to the one in the first 20 cm of bed on top of the injector (equations **Error! Reference source not found.** and **Error! Reference source not found.**)), but the gradient of pressure along the bed height is not taken into account. In evaluating the simulation results, it was necessary to consider not only bulk density and height but the qualitative behaviour of the bed too. Also, typical porosities of aerated FCC beds are usually between 0.35 and 0.5 [57] so, considering that the solid is coming out of a cyclone dipleg and that the flow is going to be more concentrated, it is possible that the experimental fraction was higher than 0.4.

Due to these factors, it was thought to lead a study on the solid volume fraction at the top inlet, for which three fractions were used ($\varepsilon_s = 0.4, 0.5, 0.55$) and the results are shown in Figure 7.6 and Figure 7.7. From the graphs, a fraction comprised between 0.5 and 0.55 seems to fit fairly well the bulk density, although for the height the results are all comparable and far from the experiments, with the fraction at 0.5 being the closest.

$$\Delta P = \rho \cdot \varepsilon_s \cdot g \cdot \Delta h \tag{45}$$

$$\Delta h = \frac{\Delta P}{\rho \cdot \varepsilon_s \cdot g} \tag{46}$$

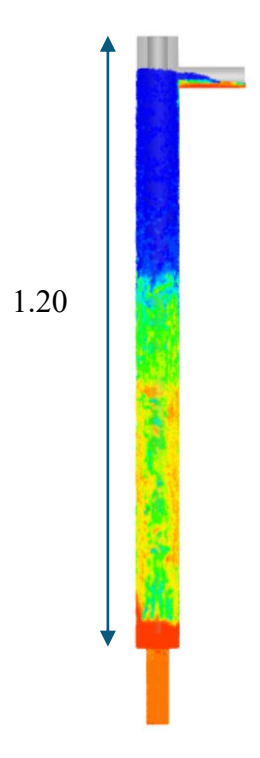


Figure 7.5: Bed hydrodynamics for $\varepsilon_s = 0.4$ at time 150s

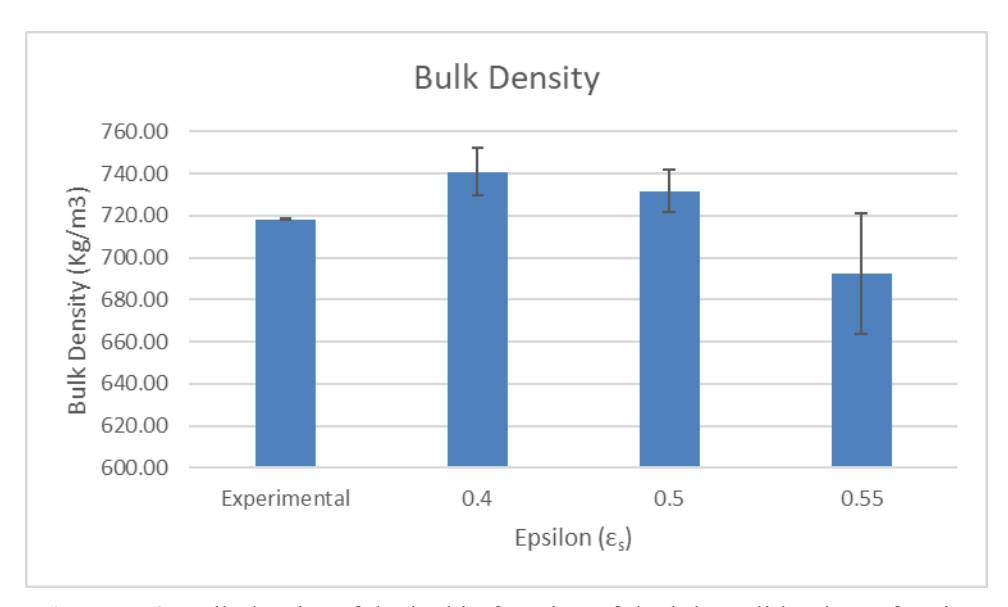


Figure 7.6: Bulk density of the bed in function of the inlet solid volume fraction

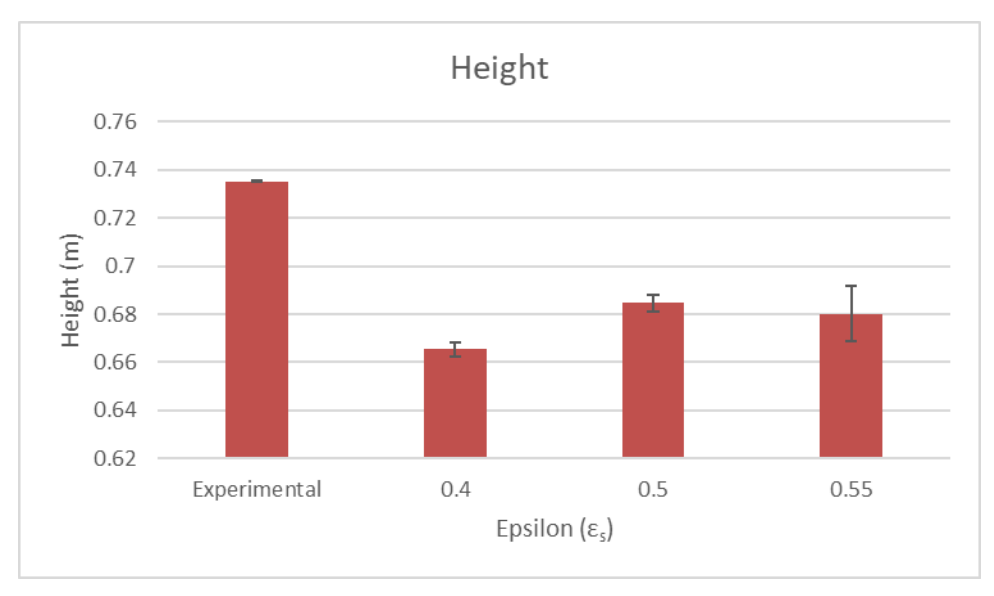


Figure 7.7: Height of the bed in function of the inlet solid volume fraction

Figure 7.6 shows a decrease in the bulk density of the bed that is paired with an increase in the bed height shown in Figure 7.7. Intuitively, an increase of the density was expected due to the higher solid concentration, so two hypotheses have been put forward. The first one suggests that the higher particles' number obstacles better the passage of the air from the injectors towards the top of the unit, meaning that a bigger amount of air occupies the volume together with the solid, lowering the bulk density and expanding the particles to the top. The second hypothesis, instead, suggests that the higher solid concentration obstacles the passage towards the top outlet of the gas mixture coming from the dipleg. In this way the two gas flows (the one from the dipleg and the one from the injectors) would impact on one another, decreasing the density and expanding the bed.

Further analysis needs to be pursued on the matter, for example by a study on the radial distribution of the gas in the vessel which would confirm the first hypothesis in the case of a greater gas concentration at the sides of the column for a lower ε_s (easier formation of preferential pathways at lower solid fraction).

7.3.3 Momentum Retention Parameters

Particle-wall interactions can play an important role in the determination of the column hydrodynamics. The use of a free slip condition (MRP \rightarrow 1) at the wall is usually suggested in literature and especially for coarse grids [50].

The FCC catalyst has been considered as a hard particle and therefore the same value has been chosen for the normal and tangential parameters. The MRP have been tested for values of 0.2, 0.5, and 1 and the results compared with experimental in Figure 7.8 and Figure 7.9.

The graphs show a trend similar to the one obtained for the solid volume fraction, with a decrease of the bulk density and an increase of the bed height with the increasing of the parameter value. The result was expected since an increase in the parameter means that the impact with the wall dissipates less energy, which is then going to be used to propel the particles towards the top of the bed and leave a lower concentration overall.

The results concerning the height present the same problem already discussed in section 7.3.2 and, in particular, when a lower momentum retention is assigned to particles, the gradient of pressure along the bed becomes steeper, leading to a greater error in the calculation. It is possible to see this in Figure 7.10, where the snapshots of the reactor's fluid dynamics at 150 seconds for the different MRP are compared. Qualitatively, it is shown a more

homogeneously dispersed solid at MRP = 1, meaning that the calculated height is more reliable.

The MRP value chosen for the optimized solution is therefore the value of 1, in accordance with the experimental data and with literature.

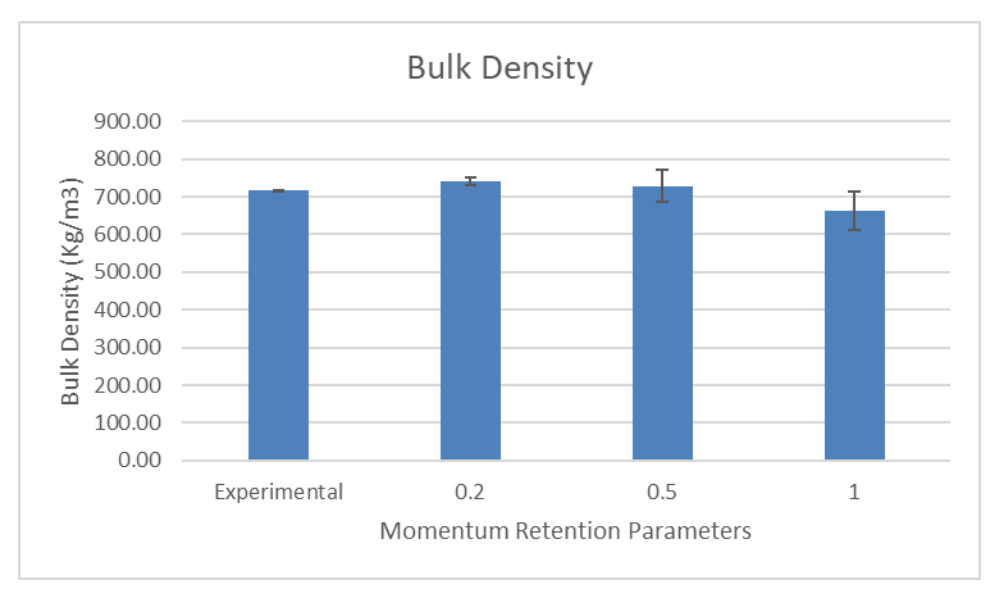


Figure 7.8: Bulk density of the bed in function of the MRP

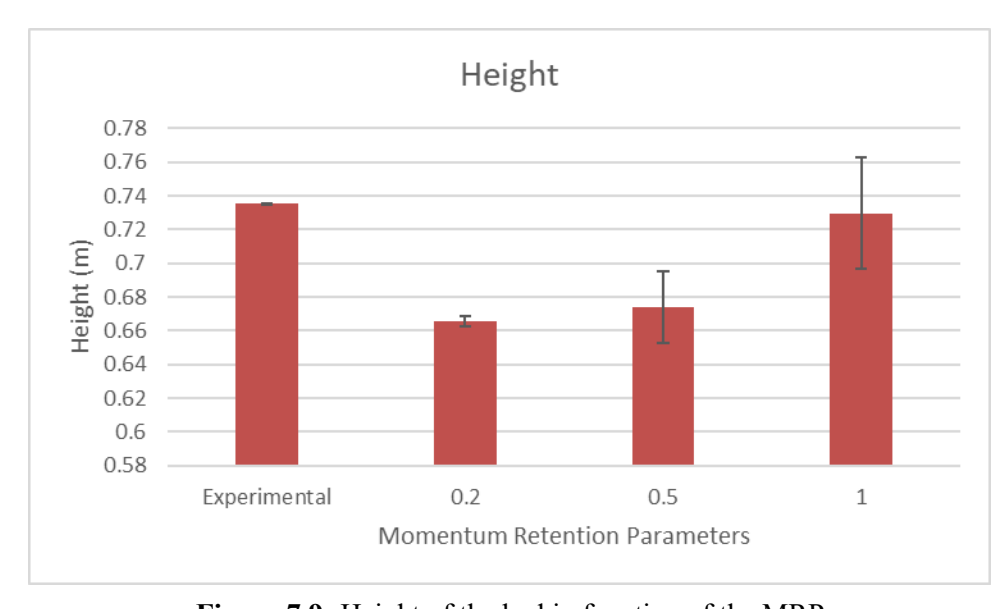


Figure 7.9: Height of the bed in function of the MRP

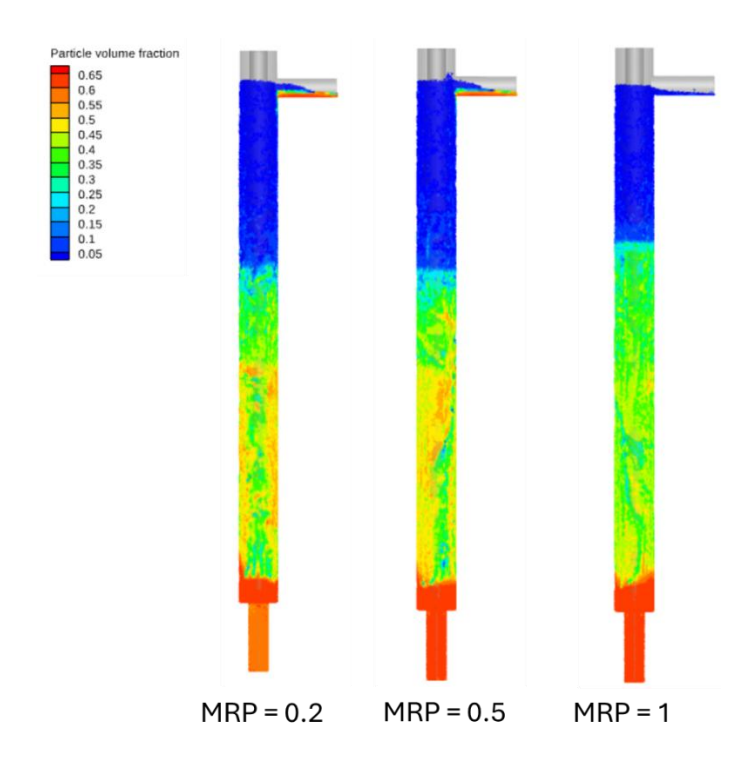


Figure 7.10: Column snapshot at 150s for different MRP values

7.4 Conclusion

Three main parameters have been observed in this sensitivity analysis: drag model, solid volume fraction of the inlet solid flow, and momentum retention parameters.

It resulted that a homogeneous drag model was able to describe the system without the need for a modification of the drag law and, given the results, the Gidaspow model seemed to better represent the fluid dynamics.

The solid volume fraction had a significant impact but with a nonobvious correlation to the results that needs to be further investigated.

The momentum retention parameters followed the expected behaviour and the condition of "free slip" at the wall seems to be the one better reproducing the experimental conditions.

Finally, the optimized simulation setup would present the Gidaspow as drag model, a solid volume fraction comprised between 0.5 and 0.55 and a MRP of 1. The combined effects of these last two parameters need to be taken into account.

8 Pulsated Inlet Simulation

This last section is dedicated to the reproduction of the experimental results with a pulsating gas inlet. Once again, the results are provided for a solid flux of $15 \text{ Kg/m}^2/\text{s}$, and the pulsation frequencies chosen are 1-3-5-7 Hz.

8.1 Methodology

Due to time constraints, the simulations with a pulsating inlet started while the data for the sensitivity analysis was still being processed, therefore, the simulation setup, which is going to be described in the following section, is not the optimized one.

A pulsating inlet was implemented, via a modification of the injection boundary conditions, reproducing the on/off type of input from a solenoid valve.

Finally, the results from the bed bulk density, height and stripping efficiency are going to be compared with the trends found at IFPEN.

8.2 Simulation Setup

The setup taken into consideration is the same one as the final case of section 7.2.3 but with an ε_s equal to 0.5.

For completeness, in the following table, the simulation boundary conditions are reported.

Table 9: Boundary Conditions for Pulsated Inlet Simulations

Boundary Conditions

Air Injection	Injection BC
	• 21 injection points distributed as in Figure 7.2
	• Air velocity equal to 13.477 m/s
	• Air mass flow equal to 2.917E-5 Kg/s
	• Frequencies: 1-3-5-7 Hz
Particle Inlet	Flow BC
	• Composition: 0.5 particles + 0.5 gas mixture (Helium + air)
	Solid
	• $\dot{m}_s = 0.075398 Kg/s$
	Fluid
	• $m_{tot} = 1.1250E - 4 Kg/s$
	• $\%_{\text{wt}}$ air = 0.97554 and $\%_{\text{wt}}$ He = 0.02446
Particle Outlet	Flow BC
	Solid
	 Outflow with size volume filtering (no size limitation)
	• Target solid flowrate = -0.075398 Kg/s
	• Target particle volume fraction (ε) = 0.6
	Fluid
	• Exit velocity = 0 m/s
	• Air mass fraction = 1 (not influent on exit composition)
Top Outlet	Pressure BC
	Solid

• Outflow with size volume filtering (no size limitation)

Fluid

- Pressure = 1 bar
- Temperature = 300 K
- Air mass fraction = 1 (not influent on exit composition)

8.3 Results

Figure 8.1 and Figure 8.2 show the bulk density and the height of the bed in function of the pulsation frequency, and in comparison with the experimental data. Looking at the simulation results, very little variation is shown from the continuous case, both for density and height; the modest trend traced by the dots suggests a slight increase in density for the frequencies in the low range, which return to the same levels as the continuous case for higher frequencies, while the opposite is true for the height graph. Although the tendency of fluidized bed properties to get closer to the value of the continuous case has already been noticed in literature [45], the results obtained are far from the ones obtain experimentally and tracing opposite trends, if compared to them.

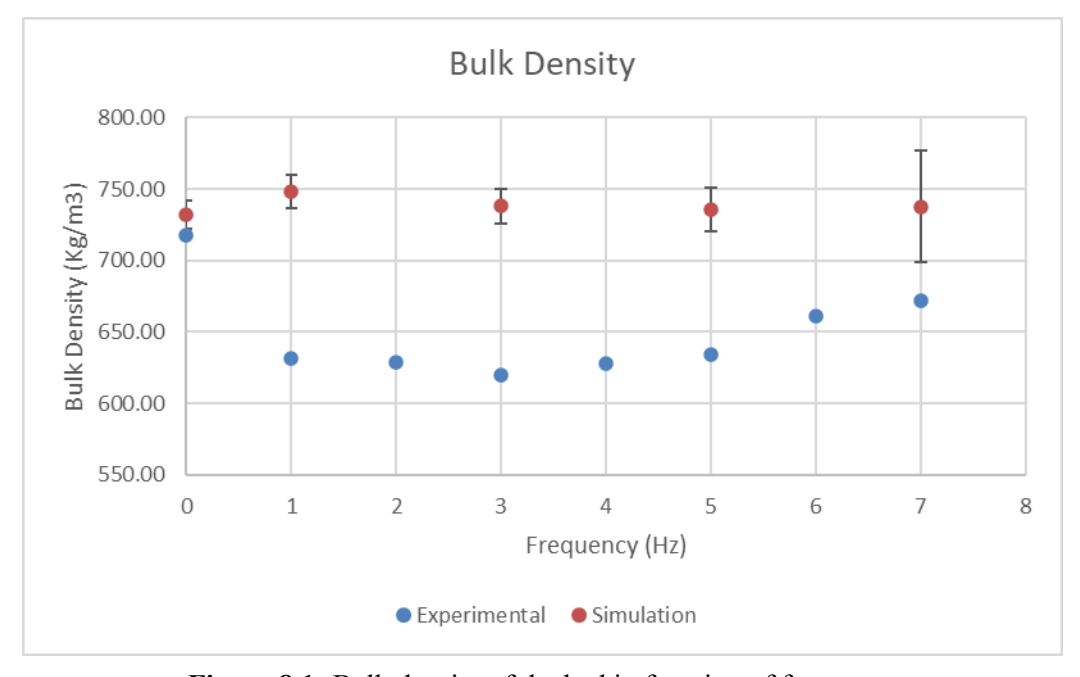


Figure 8.1: Bulk density of the bed in function of frequency

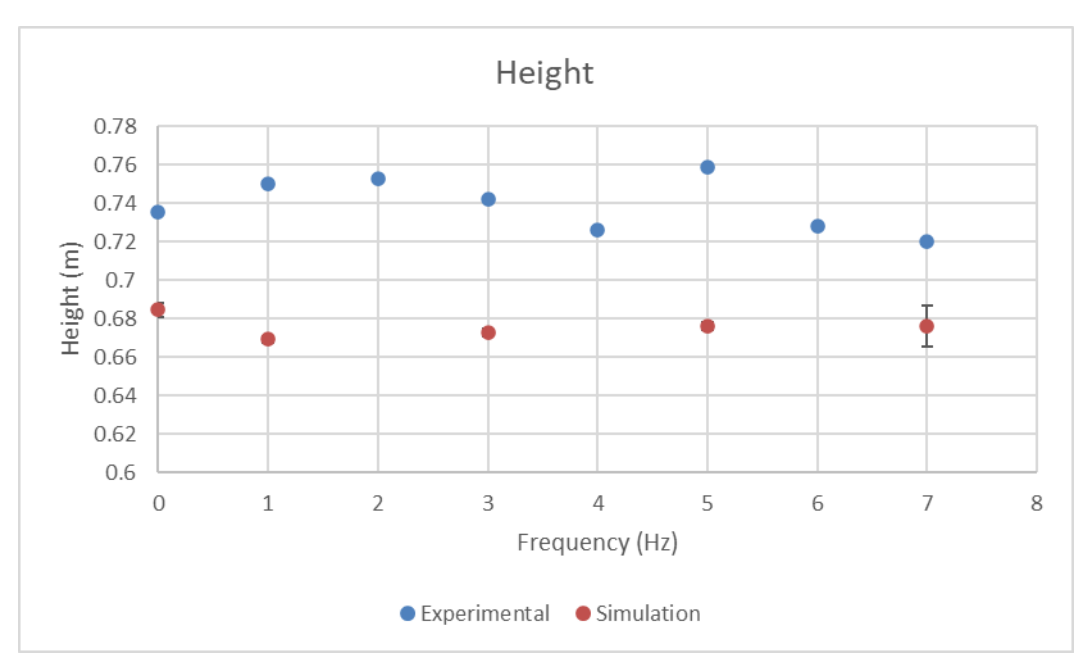


Figure 8.2: Height of the bed in function of frequency

Figure 8.3 shows the mass fraction of Helium exiting from the top outlet of the vessel, normalized in function of the Helium mass fraction from the continuous case. It is interesting to notice that, despite the difference in the representation of the hydrodynamics of the bed, the stripping efficiency seems to follow the same curve as the experimental one. It shows an increase for the frequencies in the intermediate range (from 1 to 5 Hz) and a successive decrease at higher ones.

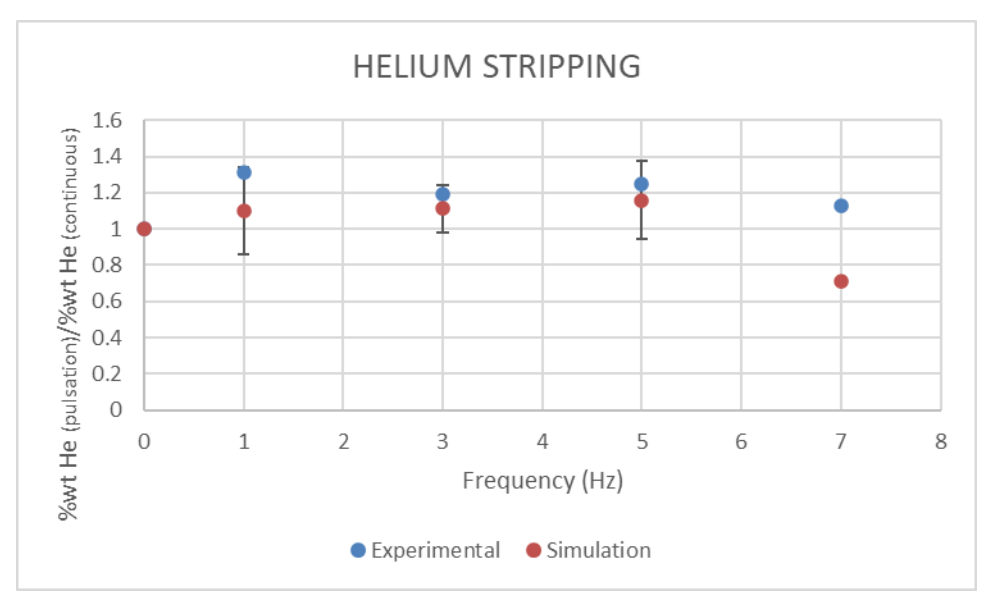


Figure 8.3: Bulk density of the bed in function of frequency

8.4 Conclusion

The impact of four inlet gas frequencies on the hydrodynamics and stripping efficiency of Helium has been tested. The bed bulk density and height results have shown trends far from the experimental ones and a little effect overall of the pulsation of the gas, while better results have been obtained for the calculation of the stripping efficiency.

In conclusion, a further study on the matter is necessary and the use of the optimized model coming from the sensitivity analysis should be useful in the resolution of the problems related to hydrodynamics. The increase in the number of simulated frequencies to match the experimental ones and the representation of the density in function of the bed height might provide some useful insight for the trouble shooting.

9 Conclusions

In this report, the results obtained during the internship in IFP Energies Nouvelles have been described. To summarize, at first a systematic literature review was conducted to analyse the advancement and interest of research on the topic and retrieve important information related to the models and simulation parameters used for fluidized beds of Geldart A particles with a pulsating inlet. Secondly, starting from the work already performed at IFPEN, a pilot scale fluidized bed stripper has been represented numerically with the use of the MP-PIC approach in order to test its capacity to reproduce the experimental data.

In section 6, the research process and its results have been described. It was reported a scarce quantity of studies, mainly focused on other types of particles that show better fluidization behaviour than the Geldart A ones. The articles under review showed a good agreement regarding computational model and parameter choice. In the end, the quasi-totality of the papers used a Eulerian-Eulerian approach with the Two Fluid Model, leaving the application of Eulerian-Lagrangian approaches to beds of aeratable particles as a field with little to no literature on it and still to be explored.

In sections 7 and 8, a CPFD model of the bed has been created and a study has been made for its optimization and accuracy with respect to the experimental data available and on the basis of the information gained in the literature review. In the first section, a sensitivity analysis has been performed on three of the most influential parameters of the simulation: drag model, inlet solid volume fraction and momentum retention parameters. The analysis showed that by varying these parameters it was possible to obtain an accurate description of the fluid dynamics of the bed and a reliable model for a future representation of different flow conditions. The model is currently not available, but under processing.

The representation of pulsation showed encouraging results especially regarding the increasing stripping capabilities of the pulsating inlet, that were in accordance with the experiments. Although, the model failed in reproducing the flow characteristics which were not presenting a big difference from the continuous case and trends quite different from the experimental ones. The use of a non-optimized model is currently the main factor, but a more in-depth analysis of the results has to be carried out to have a better view of the results.

In conclusion, the simulations show encouraging results, for this reason the prosecution of the work with the MP-PIC approach is suggested. On one side, a more extended study of the simulation parameters impact is advised, such as the use of two different values for the MRP or a greater attention to the coefficients of the stress tensor. On the other side, a deeper understanding of physics is also needed and the prosecution of lab scale experiments and the repetition of these experiments at different operating conditions, such as a higher solid flux inside the stripper, are recommended.

9.1 Future Perspectives

The future work comprises the finalization of the optimized setup, therefore finding the most appropriate solid volume fraction to fit the data.

Consequently, an analysis of the stripping efficiency at the four frequencies (1-3-5-7 Hz) and for two solid mass flux conditions (15 and 32 Kg/m³/s) has to be performed to complete the study.

Finally, an in-depth study of the results will be conducted, focused on the pressure drop along the column, the gas velocity as a function of height and radial distance, and the Helium concentration profiles throughout the height and the diameter of the bed.

10 Bibliography

- [1] Rigutto M.S., van Veen R., Huve L. Chapter 24 Zeolites in Hydrocarbon Processing, in *Studies in Surface Science and Catalysis: Introduction to Zeolite Science and Practice*. Éd. J. Čejka, H. van Bekkum, A. Corma, F. Schüth. Elsevier, 2007, 855-XXVI.
- [2] Fluid catalytic cracking process description—converter section, in *Fluid Catalytic Cracking Handbook*. Elsevier, 2020, 1-22.
- [3] Market Realist. What Is Crude Oil Refining and How Does It Work?https://marketrealist.com/2016/11/crude-oil-refining/, consulté 3 septembre 2025.
- [4] Corma A., Martínez A. Zeolites in refining and petrochemistry.
- [5] Wikipedia. Fluid catalytic cracking.https://en.wikipedia.org/w/index.php?title=Fluid_catalytic_cracking&oldid=130057143 4, consulté 7 septembre 2025.
- [6] Akah A., Al-Ghrami M. Maximizing propylene production via FCC technology, *Applied Petrochemical Research*, 2015, **5**, 4, 377-392. DOI: 10.1007/s13203-015-0104-3.
- [7] Cocco R., Chew J.W. 50 years of Geldart classification, *Powder Technology*, 2023, **428**, 118861. DOI: 10.1016/j.powtec.2023.118861.
- [8] Zhang J., Zhang X. The thermochemical conversion of biomass into biofuels.
- [9] Francia V., Wu K., Coppens M.-O. Dynamically structured fluidization: Oscillating the gas flow and other opportunities to intensify gas-solid fluidized bed operation, *Chemical Engineering and Processing Process Intensification*, 2021, **159**, 108143. DOI: 10.1016/j.cep.2020.108143.
- [10] Hoque M.M., Joshi J.B., Evans G.M., Mitra S. A critical analysis of turbulence modulation in particulate flow systems: a review of the experimental studies, *Reviews in Chemical Engineering*, 2024, **40**, 4, 511-544. DOI: 10.1515/revce-2022-0068.
- [11] Ireland E., Pitt K., Smith R. A review of pulsed flow fluidisation; the effects of intermittent gas flow on fluidised gas—solid bed behaviour, *Powder Technology*, 2016, **292**, 108-121. DOI: 10.1016/j.powtec.2016.01.018.
- [12] Tameson.com. Solenoid Valve Response Time Explained.https://tameson.com/pages/solenoid-valve-response-time, consulté 25 juillet 2025.
- [13] Kunii D. Fluidization engineering. Butterworth-Heinemann, Boston, 1991, 491 p.
- [14] Khosravi Bizhaem H., Basirat Tabrizi H. Experimental study on hydrodynamic characteristics of gas—solid pulsed fluidized bed, *Powder Technology*, 2013, **237**, 14-23. DOI: 10.1016/j.powtec.2013.01.001.
- [15] Nishimura A., Deguchi S., Matsuda H., Hasatani M., Mujumdar A.S. Heat transfer characteristics in a pulsating fluidized bed in relation to bubble characteristics, *Heat Transfer—Asian Research*, 2002, **31**, 4, 307-319. DOI: 10.1002/htj.10038.
- [16] Köksal M., Vural H. Bubble size control in a two-dimensional fluidized bed using a moving double plate distributor, *Powder Technology*, 1998, **95**, 3, 205-213. DOI: 10.1016/S0032-5910(97)03337-8.
- [17] Zhang D., Koksal M. Heat transfer in a pulsed bubbling fluidized bed, *Powder Technology*, 2006, **168**, 1, 21-31. DOI: 10.1016/j.powtec.2006.06.017.
- [18] Hadi B., van Ommen J.R., Coppens M.-O. Enhanced Particle Mixing in Pulsed Fluidized Beds and the Effect of Internals, *Industrial & Engineering Chemistry Research*, 2012, **51**, 4, 1713-1720. DOI: 10.1021/ie200933k.
- [19] Akhavan A., van Ommen J.R., Nijenhuis J., Wang X.S., Coppens M.-O., Rhodes M.J. Improved Drying in a Pulsation-Assisted Fluidized Bed, *Industrial & Engineering Chemistry Research*, 2009, **48**, 1, 302-309. DOI: 10.1021/ie800458h.
- [20] Reyes A., Campos C., Vega R. Drying of Turnip Seeds with Microwaves in Fixed and Pulsed Fluidized Beds, *Drying Technology*, 2006, **24**, 11, 1469-1480. DOI: 10.1080/07373930600952818.
- [21] Jezowska A. KINETICS OF DRYING IN CYCLICALLY SHIFTED SPOUTED BED, *Drying Technology*, 1993, **11**, 2, 319-337. DOI: 10.1080/07373939308916822.

- [22] Yang L., Han C., Xu J., Lu B., Xu Y., Wang W., Ge W. Role of mesoscale structure in gas–solid fluidization: Comparison between continuum and discrete approaches, *Chemical Engineering Journal*, 2023, **454**, 139979. DOI: 10.1016/j.cej.2022.139979.
- [23] Liang Y., Zhang Y., Li T., Lu C. A critical validation study on CPFD model in simulating gas—solid bubbling fluidized beds, *Powder Technology*, 2014, **263**, 121-134. DOI: 10.1016/j.powtec.2014.05.003.
- [24] Karimipour S., Pugsley T. Application of the particle in cell approach for the simulation of bubbling fluidized beds of Geldart A particles, *Powder Technology*, 2012, **220**, 63-69. DOI: 10.1016/j.powtec.2011.09.026.
- [25] Deen N.G., van Sint Annaland M., van der Hoef M.A., Kuipers J. Review of discrete particle modeling of fluidized beds, *Chemical Engineering Science*, 2007, **62**, 1-2, 28-44. DOI: 10.1016/j.ces.2006.08.014.
- [26] Vashisth S., Ahmadi Motlagh A.H., Tebianian S., Salcudean M., Grace J.R. Comparison of numerical approaches to model FCC particles in gas—solid bubbling fluidized bed, *Chemical Engineering Science*, 2015, **134**, 269-286. DOI: 10.1016/j.ces.2015.05.001.
- [27] Córcoles J.I., Acosta-Iborra A., Almendros-Ibáñez J.A., Sobrino C. Numerical simulation of a 3-D gas-solid fluidized bed: Comparison of TFM and CPFD numerical approaches and experimental validation, *Advanced Powder Technology*, 2021, **32**, 10, 3689-3705. DOI: 10.1016/j.apt.2021.08.029.
- [28] Snider D.M., Clark S.M., O'Rourke P.J. Eulerian–Lagrangian method for three-dimensional thermal reacting flow with application to coal gasifiers, *Chemical Engineering Science*, 2011, **66**, 6, 1285-1295. DOI: 10.1016/j.ces.2010.12.042.
- [29] Massaro Sousa L., Amblard B., Tebianian S. CFD simulation for characterization and scale-up of pulsed biomass transport, *Chemical Engineering Science*, 2022, **255**, 117652. DOI: 10.1016/j.ces.2022.117652.
- [30] Gao X., Li T., Sarkar A., Lu L., Rogers W.A. Development and validation of an enhanced filtered drag model for simulating gas-solid fluidization of Geldart A particles in all flow regimes, *Chemical Engineering Science*, 2018, **184**, 33-51. DOI: 10.1016/j.ces.2018.03.038.
- [31] CPFD Inc. Barracuda User Manual.
- [32] Yohana E., Muchammad, Tauviqirrahman M., Sayekti A.A., Choi K.-H., Paramita V. Effect of particle size and bed height on the characteristic of a fluidized bed dryer, *Cogent Engineering*, 2020, 7, 1, 1738185. DOI: 10.1080/23311916.2020.1738185.
- [33] Gidaspow D. Hydrodynamics of Fiuidization and Heat Transfer: Supercomputer Modeling, *Applied Mechanics Reviews*, 1986, **39**, 1, 1-23. DOI: 10.1115/1.3143702.
- [34] Yang N., Wang W., Ge W., Li J. CFD simulation of concurrent-up gas—solid flow in circulating fluidized beds with structure-dependent drag coefficient, *Chemical Engineering Journal*, 2003, **96**, 1-3, 71-80. DOI: 10.1016/j.cej.2003.08.006.
- [35] Particle-fluid two-phase flow: the energy-minimization multi-scale method, 1994.
- [36] Tenneti S., Garg R., Subramaniam S. Drag law for monodisperse gas—solid systems using particle-resolved direct numerical simulation of flow past fixed assemblies of spheres, *International Journal of Multiphase Flow*, 2011, **37**, 9, 1072-1092. DOI: 10.1016/j.ijmultiphaseflow.2011.05.010.
- [37] Beetstra R., van der Hoef M.A., Kuipers J.A. M. Drag force of intermediate Reynolds number flow past mono- and bidisperse arrays of spheres, *AIChE Journal*, 2007, **53**, 2, 489-501. DOI: 10.1002/aic.11065.
- [38] Radl S., Sundaresan S. A drag model for filtered Euler-Lagrange simulations of clustered gasparticle suspensions, *Chemical Engineering Science*, 2014, **117**, 416-425. DOI: 10.1016/j.ces.2014.07.011.
- [39] Shuai W., Zhenhua H., Huilin L., Yunchao Y., Pengfei X., Guodong L. Hydrodynamic modeling of particle rotation in bubbling gas-fluidized beds, *International Journal of Multiphase Flow*, 2012, **39**, 159-178. DOI: 10.1016/j.ijmultiphaseflow.2011.09.007.
- [40] Zhong H., Lan X., Gao J., Zheng Y., Zhang Z. The difference between specularity coefficient of 1 and no-slip solid phase wall boundary conditions in CFD simulation of gas—solid fluidized beds, *Powder Technology*, 2015, **286**, 740-743. DOI: 10.1016/j.powtec.2015.08.055.

- [41] Li T., Grace J., Bi X. Study of wall boundary condition in numerical simulations of bubbling fluidized beds, *Powder Technology*, 2010, **203**, 3, 447-457. DOI: 10.1016/j.powtec.2010.06.005.
- [42] Shah M.T., Utikar R.P., Pareek V.K. CFD study: Effect of pulsating flow on gas—solid hydrodynamics in FCC riser, *Particuology*, 2017, **31**, 25-34. DOI: 10.1016/j.partic.2016.07.002.
- [43] Derouin C., Nevicato D., Forissier M., Wild G., Bernard J.-R. Hydrodynamics of Riser Units and Their Impact on FCC Operation, *Industrial & Engineering Chemistry Research*, 1997, **36**, 11, 4504-4515. DOI: 10.1021/ie970432r.
- [44] Chaiwang P., Chitcharoenyoo H., Piumsomboon P., Chalermsinsuwan B. Effect of a pulsating flow on hydrodynamics and fluid catalytic cracking chemical reaction in a circulating fluidized bed riser, *Particuology*, 2022, **67**, 47-56. DOI: 10.1016/j.partic.2021.10.002.
- [45] Xiaoxue J., Shuyan W., Zhenguang L., Marcellus U.U., Baoli S., Huilin L. Pulsation active method-based particle cluster regulation using dynamic cluster structure-dependent drag model in a fluidized bed riser, *Chemical Engineering Science*, 2022, **249**, 117370. DOI: 10.1016/j.ces.2021.117370.
- [46] Dubrawski K., Tebianian S., Bi H.T., Chaouki J., Ellis N., Gerspacher R., Jafari R., Kantzas A., Lim C., Patience G.S., Pugsley T., Qi M.Z., Zhu J.X., Grace J.R. Traveling column for comparison of invasive and non-invasive fluidization voidage measurement techniques, *Powder Technology*, 2013, 235, 203-220. DOI: 10.1016/j.powtec.2012.10.031.
- [47] Wei F., Lin H., Cheng Y., Wang Z., Jin Y. Profiles of particle velocity and solids fraction in a high-density riser, *Powder Technology*, 1998, **100**, 2-3, 183-189. DOI: 10.1016/S0032-5910(98)00139-9.
- [48] Andreux R., Petit G., Hemati M., Simonin O. Hydrodynamic and solid residence time distribution in a circulating fluidized bed: Experimental and 3D computational study, *Chemical Engineering and Processing Process Intensification*, 2008, 47, 3, 463-473. DOI: 10.1016/j.cep.2007.01.023.
- [49] Gidaspow D. Multiphase Flow and Fluidization: Continuum and Kinetic Theory Descriptions. Academic Press, 1994.
- [50] Igci Y., Pannala S., Benyahia S., Sundaresan S. Validation Studies on Filtered Model Equations for Gas-Particle Flows in Risers, *Industrial & Engineering Chemistry Research*, 2012, **51**, 4, 2094-2103. DOI: 10.1021/ie2007278.
- [51] Mehrabadi M., Murphy E., Subramaniam S. Development of a gas-solid drag law for clustered particles using particle-resolved direct numerical simulation, *Chemical Engineering Science*, 2016, **152**, 199-212. DOI: 10.1016/j.ces.2016.06.006.
- [52] WEN C. Y. Mechanics of Fluidization, Fluid Particle Technology, Chem. Eng. Progress. Symposium Series, 1966, 62, 100-111.
- [53] Shi Z., Wang W., Li J. A bubble-based EMMS model for gas—solid bubbling fluidization, *Chemical Engineering Science*, 2011, **66**, 22, 5541-5555. DOI: 10.1016/j.ces.2011.07.020.
- [54] Hong K., Shi Z., Wang W., Li J. A structure-dependent multi-fluid model (SFM) for heterogeneous gas—solid flow, *Chemical Engineering Science*, 2013, **99**, 191-202. DOI: 10.1016/j.ces.2013.05.050.
- [55] Motlagh A.A., Grace J.R., Salcudean M., Hrenya C.M. New structure-based model for Eulerian simulation of hydrodynamics in gas–solid fluidized beds of Geldart group "A" particles, *Chemical Engineering Science*, 2014, **120**, 22-36. DOI: 10.1016/j.ces.2014.08.042.
- [56] Córcoles J.I., Acosta-Iborra A., Almendros-Ibáñez J.A., Sobrino C. Numerical simulation of a 3-D gas-solid fluidized bed: Comparison of TFM and CPFD numerical approaches and experimental validation, *Advanced Powder Technology*, 2021, **32**, 10, 3689-3705. DOI: 10.1016/j.apt.2021.08.029.
- [57] Abdullah E.C., Geldart D. The use of bulk density measurements as flowability indicators, *Powder Technology*, 1999, **102**, 2, 151-165. DOI: 10.1016/S0032-5910(98)00208-3.

11 List of Figures

Figure 2.1: Refining process cuts and final products [3]	12
Figure 2.2: FCC Scheme [4]	
Figure 2.3: FCC catalyst [5]	13
Figure 2.4 : Geldart Classification [6]	13
Figure 2.5: Different regimes of fluidization for a fluidized bed [9]	15
Figure 2.6: Process intensification methods for fluidized beds [8]	16
Figure 2.7: Pressure drop behaviour in fluidized beds [12]	17
Figure 2.8: Particle displacement in function of pulsation frequency [16]	19
Figure 2.9: qualitative analysis of mixing performance of wet Geldart B particles: Continuous flow vs	
3Hz flow [18]	20
Figure 2.10: P&ID of the circulating fluidized bed	23
Figure 2.11: lateral and frontal view of the stripper	
Figure 2.12: Gas sparger with dimensions	24
Figure 2.13: results of He tests with average values at 32 kg/m ² /s	26
Figure 3.1: Balance of forces on the particle [30]	30
Figure 3.2: Model for momentum retention	35
Figure 3.3: Angle variation in function of the Diffuse Bounce	35
Figure 5.1 : Sankey Diagram of the Research Results	
Figure 5.2	40
Figure 5.3	40
Figure 5.4	41
Figure 5.5	41
Figure 5.6: Cluster diameter, solid volume fraction, existence time fraction, and number fraction in	
function of different pulsation frequencies. [43]	42
Figure 5.7: Cluster diameter, solid volume fraction, existence time fraction, and number fraction in	
function of the amplitude of pulsation at a fixed frequency of 8 Hz. [43]	
Figure 5.8: Impact of drag model on time-averaged axial profiles of bed void fraction	44
Figure 5.9: Predicted expansion heights for the bubbling fluidized bed in function of the drag model	
Figure 6.1: Geometry and Boundary Conditions of the simulated bed.	
Figure 6.2: Details of the geometry and mesh of the sparger	
Figure 6.3: Bulk density of the bed in function of the drag model	
Figure 6.4: Height of the bed in function of the drag model	
Figure 6.5: Bed hydrodynamics for $\varepsilon_s = 0.4$ at time 150s	
Figure 6.6: Bulk density of the bed in function of the inlet solid volume fraction	
Figure 6.7: Height of the bed in function of the inlet solid volume fraction	
Figure 6.8: Bulk density of the bed in function of the MRP	
Figure 6.9: Height of the bed in function of the MRP	
Figure 6.10: Column snapshot at 150s for different MRP values	
Figure 7.1: Bulk density of the bed in function of frequency	
Figure 7.2: Height of the bed in function of frequency	
Figure 7.3: Bulk density of the bed in function of frequency	59

12 List of Tables

Table 1: Properties and PSD of the catalyst particles.21Table 2: Properties of the air at the injector and of the Helium at the solid inlet.21Table 3: Stripper's geometric characteristics.22Table 4: Bed density at different frequencies for a solid flux of 15 kg/m²/s.25Table 5: Bed height at different frequencies for a solid flux of 15 kg/m²/s.25Table 6: Helium fraction at the top exit of the stripper.25Table 7: Pilot scale reactor dimensions.47Table 8: Boundary Conditions50		
Table 3: Stripper's geometric characteristics. Table 4: Bed density at different frequencies for a solid flux of 15 kg/m²/s. Table 5: Bed height at different frequencies for a solid flux of 15 kg/m²/s. Table 6: Helium fraction at the top exit of the stripper. Table 7: Pilot scale reactor dimensions.	Table 1: Properties and PSD of the catalyst particles	21
Table 4: Bed density at different frequencies for a solid flux of 15 kg/m²/s	Table 2: Properties of the air at the injector and of the Helium at the solid inlet	21
Table 5: Bed height at different frequencies for a solid flux of 15 kg/m²/s. 25 Table 6: Helium fraction at the top exit of the stripper. 25 Table 7: Pilot scale reactor dimensions. 47	Table 3: Stripper's geometric characteristics.	22
Table 5: Bed height at different frequencies for a solid flux of 15 kg/m²/s. 25 Table 6: Helium fraction at the top exit of the stripper. 25 Table 7: Pilot scale reactor dimensions. 47	Table 4: Bed density at different frequencies for a solid flux of 15 kg/m ² /s	25
Table 7: Pilot scale reactor dimensions		
Table 7: Pilot scale reactor dimensions	Table 6: Helium fraction at the top exit of the stripper.	25
Table 8: Boundary Conditions	* **	
	Table 8: Boundary Conditions	50